Soft Matter

Cite this: *Soft Matter*, 2012, **8**, 5728

www.rsc.org/softmatter

REVIEW

Mechanics of morphological instabilities and surface wrinkling in soft materials: a review

Bo Li,[a] Yan-Ping Cao,[a] Xi-Qiao Feng*[ab] and Huajian Gao[c]

Received 3rd January 2012, Accepted 21st February 2012
DOI: 10.1039/c2sm00011c

Morphological instabilities and surface wrinkling of soft materials such as gels and biological tissues are of growing interest to a number of academic disciplines including soft lithography, metrology, flexible electronics, and biomedical engineering. In this paper, we review some of the recent progresses in experimental and theoretical investigations of instabilities that lead to the emergence and evolution of surface wrinkling, folding and creasing under various geometrical constraints (*e.g.*, thin films, sheets, fibers, particles, tubes, cavities, vesicles and capsules) and loading stimuli (*e.g.*, mechanical forces, growth, atrophy, swelling, shrinkage, van der Waals interactions). Some representative theoretical and numerical approaches aimed at modelling the onset of instabilities as well as the postbuckling evolution involving multiple bifurcations and symmetry-breakings are discussed along with the main characteristics and some possible applications of this rich phenomenon.

1. Introduction

Soft materials such as elastomers, polymeric gels and biological tissues can easily undergo large deformation and various morphological stabilities in response to environmental stimuli (*e.g.*, mechanical forces, temperature, humidity, pH value, electric field and van der Waals interactions).[1–12] The stimulus-sensitive property of soft materials makes them promising candidates for applications as intelligent materials in therapeutics, sensors, microfluidic systems, nanoreactors, and biological scaffolds.[2]

Due to their intrinsic features of low elastic moduli and high sensitivity to external stimuli, soft materials are especially susceptible to buckling induced surface instabilities. For example, various regular or irregular wrinkles can be readily

[a]*Institute of Biomechanics and Medical Engineering, AML, Department of Engineering Mechanics, Tsinghua University, Beijing 100084, China. E-mail: fengxq@tsinghua.edu.cn; Fax: +86 10 62781824; Tel: +86 10 62772934*
[b]*Center for Nano and Micro Mechanics, Tsinghua University, Beijing 100084, China*
[c]*School of Engineering, Brown University, Providence, Rhode Island, 02912, USA*

Bo Li

Bo Li is currently a postdoctoral fellow at Johns Hopkins University. He received his B.S. degree (2004) in Engineering Mechanics and M.S. degree (2007) in Solid Mechanics from Hunan University. He obtained his Ph.D. degree in Solid Mechanics at Tsinghua University in 2011. His current research interests are focused on the morphological instability of soft materials, growth theory of biological tissue, and nonlinear elasticity. He has co-authored about 30 journal papers.

Yan-Ping Cao

Yanping Cao has been an associate professor at the Institute of Biomechanics and Medical Engineering, Tsinghua University since 2008. He earned a Ph.D. in Solid Mechanics at Tsinghua University in 2002. From 2002 to 2005, he was a postdoctoral associate at the Technology University of Troyes in France. From 2005 to 2007, he served as a Humboldt research fellow at Karlsruhe Institute of Technology and Max Planck Institute for Iron Research in Germany. His current research interests include the mechanics of biological and soft materials, contact mechanics, and computational mechanics.

observed on human skin and elastomer surfaces. Such behavior may pose a limit on the performance of materials and is often thought to be a nuisance which should be avoided.[3] On the other hand, one can also harness the physics and characteristics of wrinkles to create tunable patterns,[13–15] to fabricate functional surfaces,[16–18] to design flexible electronics,[19–21] and/or to measure the mechanical properties of materials.[22–25] Understanding the morphogenesis and the origin of shapes is also a central goal of developmental biology.[26–29] There has been a resurgence of interest in emulating and utilizing mechanical instabilities in the morphogenesis of anatomical structures, organs and organisms.[30,31] Some techniques based on the mechanical instability of surfaces have found applications in the biomedical field, *e.g.*, assisting the diagnosis and curing of certain diseases, including asthma, mucosal inflammation, gastroenteritis, and tumor invasion.[32–34]

Owing to a wide range of important applications, the problem of morphological surface instability of soft matter has attracted the attention, imagination and close scrutiny of many scientists and engineers over the past decade.[3,35] Much experimental and theoretical effort has been directed toward exploring the characteristics of surface patterns at the critical state of buckling and the subsequent postbuckling evolution, as well as understanding the underlying physical mechanisms in different types of materials.[3,23,27,36–39] Morphological instability of a soft material typically exhibits three phenotypes: wrinkling, folding, and creasing, as shown in Fig. 1. Wrinkling refers to periodic or chaotic surface undulations appearing on an originally flat surface. It is often detected during the buckling of thin structures with or without lateral supports. In a two-dimensional (2D) system, for example, a stiff film anchored on a compliant substrate may buckle into sinusoidal waves.[3] Folding refers to a buckling induced surface structure with localized, deep surface valleys. Folds are often observable, for instance, during the postbuckling evolution of surface wrinkles in a hard layer bonded to a soft substrate or floating on a liquid.[40,41] Noticeably, the term folding has been extensively adopted in fields such as biomedicine and tectonophysics to stand for traditional buckling or wrinkling.[32,42] In contrast, creasing usually occurs at the surface of soft materials without hard skins, when an initially smooth surface forms a self-contacting shape with a sharp ridge or sulci.[43–45]

Soft materials often undergo large volumetric variations due to factors such as temperature change, tissue growth/atrophy and swelling/shrinkage induced by water imbibing/release. Inhomogeneous deformation and stresses are often incurred in materials experiencing an inhomogeneous or anisotropic distribution of volumetric variations arising from structural heterogeneities, non-uniform micro-environments and/or spatial limitations in available nutrients. Constrained swelling/growth may also cause large enough compressive stresses to trigger elastic instabilities analogous to the Euler buckling induced by external mechanical loads.[3,22,35,46,47] In this paper, we review some of the recent experimental and theoretical effort toward understanding the morphological instabilities of soft materials incurred by non-uniform volumetric swelling/shrinkage or other external stimuli. The paper is outlined as follows. Section 2 briefly describes two representative models dealing with surface instability and morphological evolution in soft materials induced by swelling or growth. Sections 3–9 provide an overview of some experimental and theoretical investigations of morphological instabilities in various soft material systems including thin films, sheets, fibers, tubes, particles, cavities, vesicles and capsules. Possible applications of these results, as well as some closely related wrinkling phenomena induced by other mechanisms (*e.g.*, van der Waals interactions, electrostatic forces, and externally applied forces) will also be discussed. Finally, we offer some perspectives for future work in this rich and exciting field.

Xi-Qiao Feng

Xi-Qiao Feng is a Chang Jiang Chair Professor and the head of the Department of Engineering Mechanics, Tsinghua University. He earned a Ph.D. degree in Solid Mechanics in 1995 at Tsinghua University. From 1997 to 1999, he worked as a Humboldt research fellow in the Technical University of Darmstadt and Delft University of Technology. He rejoined Tsinghua University as an associate professor in 1999 and was promoted to a professor in 2001. Currently, he is the secretary-general of Chinese Society of Theoretical and Applied Mechanics and the director of Institute of Biomechanics and Medical Engineering. He also serves as a member of editorial board of more than 10 journals. His current interests include molecular and cellular biomechanics, mechanics of biomaterials, and fracture mechanics. He has co-authored two books and 200 journal papers.

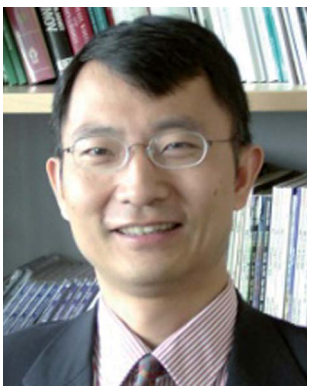

Huajian Gao

Huajian Gao is the Walter H. Annenberg Professor of Engineering at Brown University. He received his B.S. degree from Xi'an Jiaotong University in 1982, and his M.S. and Ph.D. degrees in Engineering Science from Harvard University in 1984 and 1988, respectively. He served on the faculty of Stanford University between 1988 and 2002, and was appointed a Director at the Max Planck Institute for Metals Research between 2001 and 2006. He is a Member of the National Academy of Engineering of USA and has authored or co-authored more than 300 journal papers, with total citations exceeding 11 000.

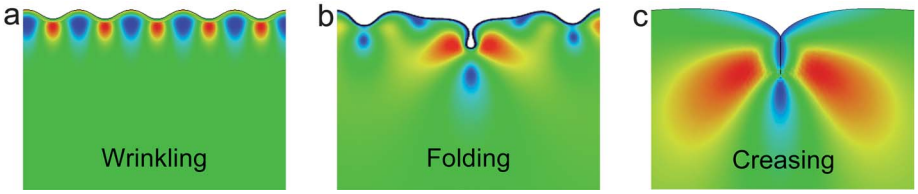

Fig. 1 Schematic of three types of morphological instability: (a) wrinkling, (b) folding, and (c) creasing.

2. Theoretical models

2.1. Growth/atrophy of living tissues

The growth or atrophy of living tissues, which usually occurs through cell division or apoptosis resulting in increase or decrease in body mass, is crucial for their physiological functions and can be subjected to various pathological disorders. Growth is responsible for the morphogenesis of biological organs and tissues, which consists of a series of carefully orchestrated steps.[48] In addition to genetic and chemical effects, mechanical environments play a significant role in regulating pattern formation. Inhomogeneous growth or atrophy of tissues and organs in a constrained environment induces internal stresses—often referred to as residual stresses—which are believed to play a significant role in the morphogenesis of tissues and organs.[27,28,49–54]

Tissue growth may take place in three typical forms, namely tip growth, surface growth, and volumetric growth.[27] In tip growth, which happens in, for instance, root hairs, fungal hyphae and pollen tubes, cells typically form a slender structure capped by a prolate dome where expansion occurs.[55–57] Surface growth is often adopted by organisms such as seashells and horn-shells, where mass tends to accrete on an existing surface.[48,58,59] In contrast, volumetric growth is responsible for the development of most soft tissues, *e.g.*, arteries, airways, heart, muscles, and solid tumors.[1,60–62] In the present paper, our attention will be focused on the morphological instability induced by volumetric growth.

In what follows, we will briefly describe a finite deformation model based on the multiplicative decomposition of the deformation gradient, analogous to the well-known decomposition of elastic and plastic deformation gradient tensors.[63] According to the pioneering work of Rodriguez *et al.*,[64] the deformation gradient tensor, $\mathbf{F}$, can be decomposed as

$$\mathbf{F} = \mathbf{F}_e \cdot \mathbf{F}_g \tag{1}$$

where $\mathbf{F}_g$ is the growth tensor describing the addition of materials, and $\mathbf{F}_e$ is the elastic deformation tensor which ensures the compatibility and integrity of the tissue.[27,48,64,65] Residual stress arises from the elastic deformation that exists to prevent discontinuities in a growing body. This decomposition can be illustrated in Fig. 2.

For the sake of simplicity, it is often assumed that the response function of a growing material depends only on the elastic part of the total deformation.[51,64] Introducing a strain energy function $W(\mathbf{F}_e)$, the nominal stress $\mathbf{S}$ can be written as[27]

$$\mathbf{S} = J\mathbf{F}_g^{-1}\left(\frac{\partial W}{\partial \mathbf{F}_e} - p\mathbf{F}_e^{-1}\right) \tag{2}$$

where $J = \det\mathbf{F}$ and p is a Lagrange multiplier associated with tissue incompressibility ($p = 0$ for a compressible soft material). The stress state of a nonlinear deformation system can also be expressed by the Cauchy stress, $\boldsymbol{\sigma} = J^{-1}\mathbf{F}\cdot\mathbf{S}$.[66] The mechanical equilibrium state induced by tissue growth or atrophy can be obtained by solving $\mathrm{Div}\mathbf{S} = 0$ or $\mathrm{div}\boldsymbol{\sigma} = 0$ together with appropriate boundary conditions, where "Div" and "div" stand for divergence operators in the initial and current configurations, respectively.[66]

When the residual stresses caused by growth are sufficiently large, they may trigger morphological instabilities in a soft material. The critical instability conditions and the induced surface wrinkling patterns can be predicted through an incremental theory of deformation, following Biot[67] and Ogden.[66] Ben Amar and Goriely incorporated the effect of tissue growth into such a theory.[27] Recently, Li *et al.*[33] adopted a similar approach to study the mucosal wrinkling driven by volumetric growth. The stability condition was determined by solving the incremental equilibrium equation $\mathrm{div}\dot{\mathbf{S}}_0 = 0$ in conjunction with specified boundary conditions, where $\dot{\mathbf{S}}_0$ is the incremental nominal stress tensor.[33,68] Surface wrinkling occurs when the incremental equilibrium equation exhibits nontrivial solutions to small perturbations in the system.

Besides the approach of multiplicative decomposition described above, an additive decomposition has also been suggested by expressing the elastic strain as the difference between the total geometrical strain and the growth strain, similar to that used in thermoelastic analyses.[28,69]

2.2. Swelling/shrinkage of hydrogels

Owing to their relatively low cost, good permeability, stimulus sensitivity, biocompatibility and biodegradability, hydrogels hold great promise for important applications in a wide range of industrial and medical fields, *e.g.*, chemical separation, food preservation, optical sensing, drug delivery, and wound dressing.[2,10,70] Similar to the growth/atrophy of biological tissues

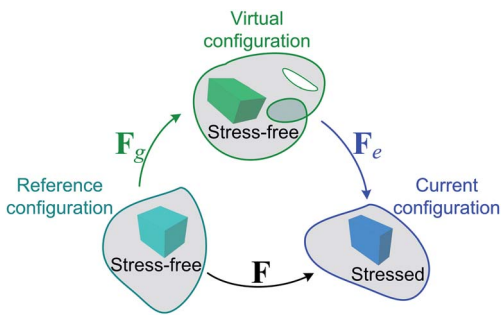

Fig. 2 Multiplicative decomposition of the deformation gradient tensor.

in animals and plants, large volumetric change due to water imbibing or drying can readily occur in hydrogels and elastomers. For example, a hydrogel is typically composed of one or more hydrophilic organic polymer components cross-linked into a network by either covalent or noncovalent interactions.[9,71,72] This network structure can swell or shrink by a huge amount in response to external stimuli such as water imbibing or dehydration. Inhomogeneous or differential swelling or shrinking due to nonuniform physical/chemical properties or physiological changes can elicit stresses and destabilize the morphology of the material.[14,39,73–75]

When elastomers or gels are immersed into a solvent, the small molecules in the solvent can migrate into the organic molecular network, engendering swelling of the material. The reverse process, *i.e.* shrinkage, occurs when the small molecules migrate out. The Helmholtz free energy density of elastomers can be expressed as a function of the deformation gradient tensor, $\mathbf{F}$, and the concentration of solvent molecules in the gel, C, that is, $W = W(\mathbf{F},C)$. At equilibrium, the chemical potential of the solvent molecules in the elastomer, defined by $\phi = \partial W/\partial C$, should be equal to that in the solvent.[9] A Legendre transformation $\hat{W} = W(\mathbf{F},C) - \phi C$ gives the related free energy density function associated with constant chemical potential.[76,77] It is often assumed that both the long polymer chains and the solvent molecules are incompressible but the polymer network is itself a compressible structure from the macroscopic perspective.[77] Thus the volume of gel is expressed as the sum of the volumes of its constituents, that is,[9]

$$1 + VC = J \tag{3}$$

where V is the volume per small solvent molecule. Employing eqn (3), the free energy function $\hat{W}$ can be rewritten as

$$\hat{W}(\mathbf{F},\phi) = W\left(\mathbf{F}, \frac{J-1}{V}\right) - \frac{\phi}{V}(J-1) \tag{4}$$

The nominal stress can be defined as $\mathbf{S} = \partial\hat{W}/\partial\mathbf{F}$. Thus the equilibrium state of the gel can be solved by following the theoretical framework of volumetric growth described in Subsection 2.1. When the free swelling of the gel is inhibited by gradient or boundary constraints, compressive stresses arise, which may trigger morphological instabilities in the system.[45,74,78] The stability condition can be derived by adopting the traditional linear perturbation method.[66,67,74,77]

As in eqn (1) and Fig. 2, the swelling of gels can also be analyzed by decomposing the deformation gradient tensor as[79–81]

$$\mathbf{F} = \mathbf{F}_e \cdot \mathbf{F}_s \tag{5}$$

where $\mathbf{F}_s$ denotes the swelling part of the deformation. The assumption that the volumetric variation arises entirely due to the change in the solvent content requires $\det\mathbf{F}_e = 1$ and $\det\mathbf{F}_s = 1 + VC = J$. In this fashion, the subsequent stability analysis can also be conducted in light of the incremental deformation theory described in Subsection 2.1.

The above theoretical models enable one to investigate the deformation and instability induced by volumetric changes. In the following sections, we review some recent experimental and theoretical advances in the morphological instabilities and surface wrinkling of soft material systems under various geometrical constraints.

3. Thin films or sheets

Freestanding thin sheets can easily lose their morphological stability and exhibit complex configurational changes in response to capillary forces,[82,83] external compression, differential or constrained swelling/shrinkage (Fig. 3a). Recently, Efrati *et al.*[69] proposed an elastic theory of thin sheets with internal growth by introducing the target metric concept. In this theory, the growth is modeled by embedding another lamella with the same elastic properties into the original sheet, leading to the so-called non-Euclidean configuration, a stressed state without any external constraint.[84–87] This approach provides an effective tool to elucidate pattern formation in freely swelling planar and curved sheets (Fig. 3b).[26,88–90]

In essence, the non-Euclidean concept is somewhat similar to an additive decomposition of the Lagrange strain tensor into an elastic strain tensor and an incompatible strain (or called intrinsic strain) tensor.[93,94] Liang and Mahadevan[28,92] utilized the additive decomposition of the Lagrange strain to investigate the role of instability in the formation of various patterns in strip-like leaves (*e.g.*, plantain lily leaves) and flowers (*e.g.*, lily), as shown in Fig. 4a and 4b. They showed that for sufficiently small growth at the edge, a global deformation with a long-wavelength saddle shape occurs. However, for larger growth at the edge, an edge-localized ripple pattern with a short wavelength occurs while the global configuration of the leaf remains almost flat. A combined mode consisting of a saddle-like shape with edge-localized ripples may appear when the edge growth is sufficiently large, as shown in Fig. 4c. In addition, it was thought that the blooming of lily flowers is driven by differential growth along the thickness of the petals and/or active curving of the midribs, while the edge-localized growth plays a crucial role in the blooming process. In artificial materials, Wang *et al.*[95] observed that under temperature-induced swelling, a polymeric strip restricted along its two edges, which may buckle into orthogonal, oblique, and crumple wrinkles (Fig. 5), depending on the strength of the edged

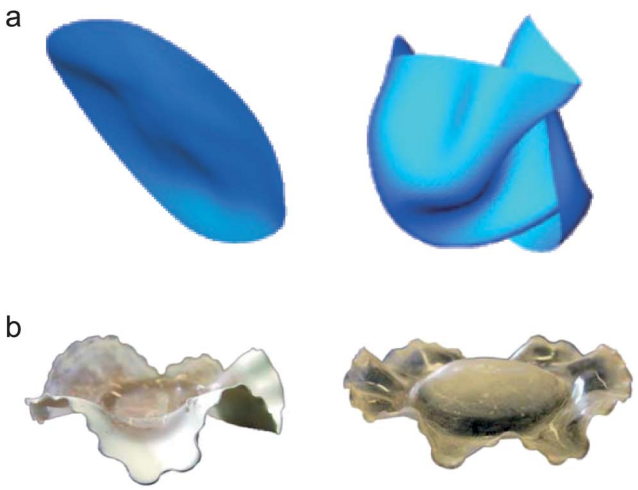

Fig. 3 (a) Flat sheets swelling in a spherical container.[91] (b) Buckling of swelling sheets.[89] Reprinted from ref. 91 and 89 with permission.

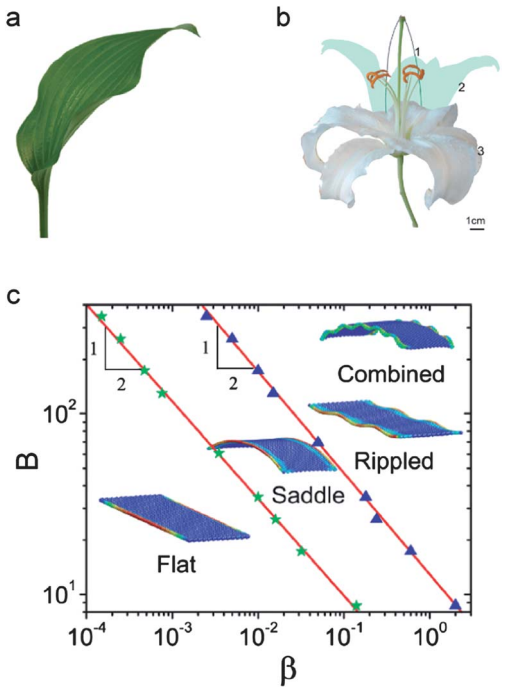

Fig. 4 Wrinkling of leaves and flowers: (a) plantain lily leaf, (b) flower of lily, and (c) diagram of pattern, where B is the width of the strip and β is the maximum growth strain at the edge of the strip.[28,92] Reprinted from ref. 28 and 92 with permission.

constraints, the temperature distribution, and the expansion properties of the strip.

Differential growth or swelling may also trigger torsional buckling in strip-like plants and engender a helical morphology with a smooth surface, as observed during the seed pod opening process in *Bauhinia variegate* (Fig. 6a).[96] Wide strips favor a configuration close to a cut from a cylindrical envelope, reminiscent of the famous Möbius strip, whereas narrow strips prefer a pure twist, where the centerline of the strip remains straight (Fig. 6b–d).[99] Nevertheless, when the strip is subjected to torsion and high longitudinal tension simultaneously, the strip may buckle into a helix with regular triangular patterns (Fig. 6e).[98] The morphology observed has a sharply curved structure with ridges running at an angle of about 45° measured from the centerline of the strip, rendering a rough surface with stress focusing similar to what appears on a crumpling paper or a gel sheet swelling in a container with limited space.[91,100]

Based on the multiplicative decomposition in eqn (1), Dervaux *et al.*[101] developed a model to describe the morphogenesis of thin

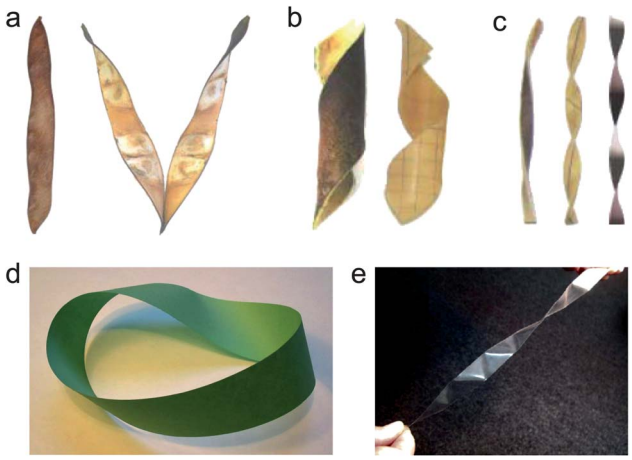

Fig. 6 Torsional buckling of strips: (a) closed and open *Bauhinia* pods, (b) cylindrical helices in wide strips, (c) twisted helices in narrow strips,[96] (d) Möbius strip,[97] and (e) twisting with high tension.[98] Reprinted from ref. 96 and 98 with permission.

sheets induced by growth or atrophy. They found that the equilibrium configuration of the sheet can be characterized by a Föppl–von Karman (FvK) type of equation where growth acts as a source of mean and Gaussian curvatures. The morphology of soft tissues with lamellate shapes, *e.g.*, plant leaves and potato chips during drying or frying, can also be explained by this theory.[51] Some researchers used the finite element method (FEM) to simulate the growth of sheet-like structures in nature.[94,102] FEM provides a versatile tool to elucidate various morphogenesis processes in nature where analytical approaches are limited. For a circular disc (*e.g.*, a lotus leaf) subjected to relatively small growth, the theoretical analysis of Dervaux and Ben Amar showed that the disc may buckle into a saddle shape when the growth in the circumferential direction is greater than that in the radial direction or a symmetric conical shape when the radial growth dominates (Fig. 7a).[51] At sufficiently large growth rates, however, FEM simulations showed that the saddle and cone shapes are no longer energetically optimal, rather the system will favor a skewed self-contact cone (Fig. 7b) featured by a skewness angle and repetitive spiral winding that allows unlimited growth.[103] Self-contacting also takes place when a thin annulus disc grows sufficiently in the circumferential direction (Fig. 7c); in this case, the threshold for the self-contact shape is contingent on the inner radius of the annulus.

Another interesting phenomenon observed in thin sheets is hierarchical or fractal wrinkles, a cascade of small waves upon larger waves, which can be seen in tearing a garbage bag

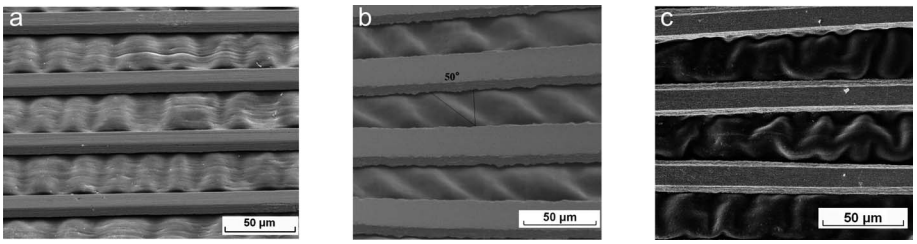

Fig. 5 Buckling of an edge-restricted strip into (a) orthogonal, (b) oblique, and (c) crumple patterns.[95] Reprinted from ref. 95 with permission.

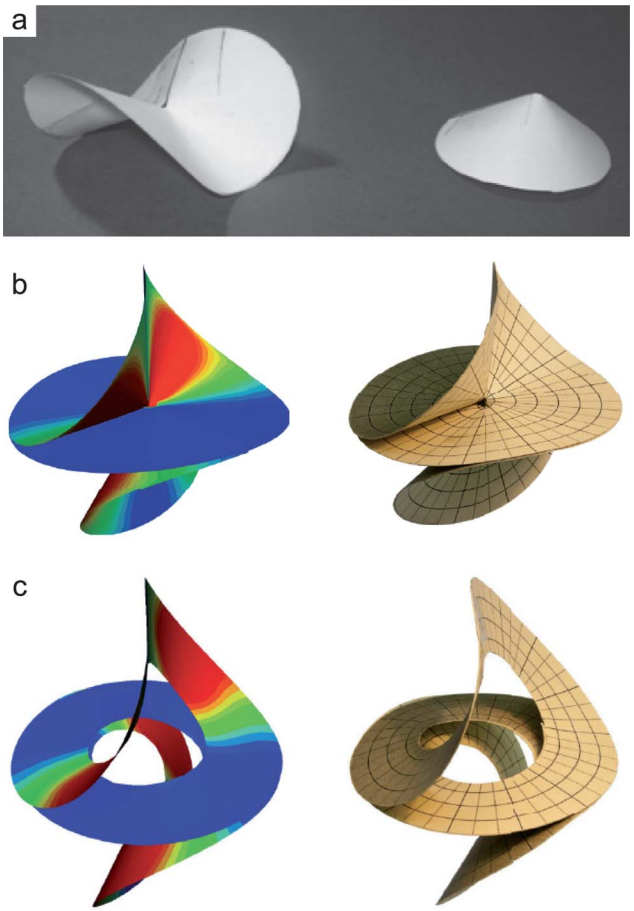

Fig. 7 Buckling of growing circular sheets: (a) buckling with or without edge oscillations,[51] (b) numerical (left) and experimental (right) results of skewed buckling in a disc, and (c) numerical (left) and experimental (right) results of skewed buckling in a ring.[103] Reprinted from ref. 51 and 103 with permission.

(Fig. 8a). Along the newly formed edges of the torn plastic sheet, patterns with up to six generations of similar waves can be found, with a scaling factor of about 3.[104,105] These patterns occur because the high plastic strain localizes at the newly formed edge when the sheet is torn; the expansive stretch leads to edge buckling in order to reduce the total potential energy of the system. Hierarchical wrinkles are also widely observed in plants. For instance, wave-on-wave structures have been found in many flower petals, lichens, and leaves (Fig. 8b) due to differential edge growth, which can be understood by invoking the buckling theory described above.[26,106]

As a parallel to the fractal wrinkles spontaneously formed at a free edge, thin elastic sheets under boundary confinement in a non-growing system may generate branching wrinkles: two wrinkles with a small wavelength merge into a single wrinkle with a larger wavelength, as shown in suspended curtains (Fig. 8c).[107,108] This phenomenon arises from the competition between stretching in the direction parallel to the wrinkles and bending along the edge.[109] The average wavelength scales as $\lambda \propto x^m$, where x denotes the distance to the constrained edge.[110–112] It is found that m is close to 2/3 for small downward dragging and 1/2 for large dragging in the direction parallel to the wrinkles.[107]

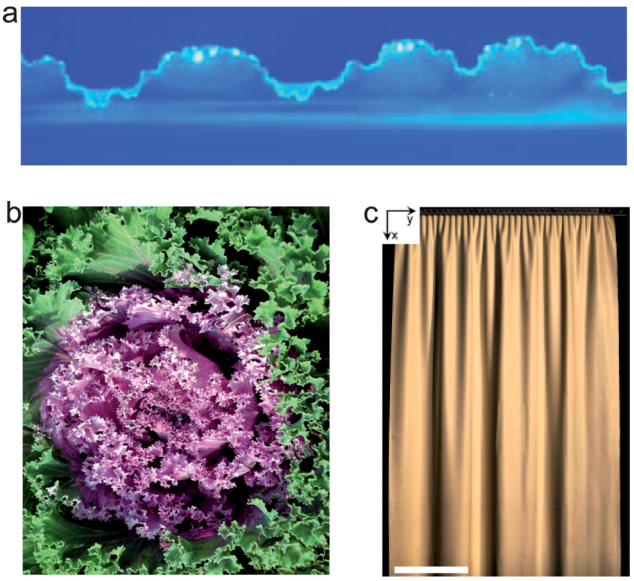

Fig. 8 Hierarchical wrinkles on (a) a torn plastic sheet,[26] (b) an ornamental cabbage, and (c) a suspended curtain.[107] Reprinted from ref. 26 and 107 with permission.

Thin sheets floating on water behave analogously to suspended curtains because the capillary force at the edge plays a similar role as downward-drag in curtains.[113]

4. Soft layers with a hard skin

Most living tissues in animals are featured by layered structures to meet their physiological and physical functions. For example, our skin, which accounts for about 16% of the body weight, comprises three layers: counting from the outer skin first comes a thin epidermis layer, followed by a thick dermis layer, and then the underlying hypodermis.[3,114] To protect the internal layers from eventual physical, biological, and chemical trauma caused by the environment, the epidermis, made of stratum corneum and keratinizing epithelial cells, is much harder than the inner layers. For the sake of simplicity, the skin is usually modeled as a stiff film resting on a compliant substrate.

As the skin ages, each layer undergoes different biological changes in the moisture content and the collagen fiber density, inducing compressive stresses in the epidermis layer. The stresses can be large enough to wrinkle the skin. Considerable attention has been attracted to the investigation of skin wrinkling and the development of possible techniques to reduce or postpone this aging process.[3,114] The epidermis layer can be described by a thin elastic plate within the FvK theoretical framework while the compliant substrate is treated as a 2D or 3D elastic continuum.[115] When the film is subjected to a sufficiently large in-plane compressive load, it wrinkles into a pattern that minimizes the total potential energy of the system. In the case of uniaxial compression, the wrinkles usually have a sinusoidal profile (Fig. 9a).[39] The wavelength, λ, can be approximately expressed as[37,116]

$$\lambda = \frac{2\pi}{3^{1/3}} h \left(\frac{\bar{E}_f}{\bar{E}_s} \right)^{1/3} \quad (6)$$

where $\bar{E} = E/(1 - v^2)$, E, and v are the plane-strain elastic modulus, Young's modulus, and Poisson's ratio of the film (f) and substrate (s), respectively, and h denotes the film thickness. This relation sheds light on the underlying competitive mechanisms: the stiffness of the film favors a larger wavelength while that of the substrate prefers a shorter wavelength. Given the mechanical properties of the system, the wavelength is proportional to the film thickness. These results also offer an effective approach to modulate surface patterns and design flexible electronics with controllable dimensions by tuning the aforementioned mechanical and geometric parameters. Additionally, the simple relation in eqn (6) opens a novel avenue for measuring the mechanical properties of thin films at the micro and nano scales, which are difficult to address with traditional methods.[22,25,117] Motivated by this, some buckling-based metrologies have been developed to characterize the elastic modulus of micro- and nanofilms/wires/tubes.[24,118,119] When subjected to biaxial compressive stresses, a thin film can buckle into different patterns, *e.g.*, checkerboard, herringbone, hexagonal, triangular, and even labyrinths patterns, as shown in Fig. 9.[36–38,120–124] The selection and mutual transition of these wrinkling modes hinge on the stress state and the loading history. When the load is equibiaxial and moderate, the herringbone pattern often appears as the mode of the lowest energy.[36,122]

Generally speaking, the theory of finite elasticity is needed to analyze layered systems with nonlinear constitutive relations and large deformation. To capture the effects of differential growth on the wrinkling of skins, consider an isotropic growth of the epidermis layer (or a shrinkage of the inner layers), that is, $\mathbf{F}_g = g\mathbf{I}$ with a constant growth rate g. Both the film and the substrate are assumed to be incompressible neo-Hookean hyperelastic materials with strain energy function $W = \mu(\alpha_1^2 + \alpha_2^2 + \alpha_3^2 - 3)/2$, where μ is the shear modulus at the ground state and α_i ($i = 1, 2, 3$) are the eigenvalues of the elastic deformation tensor. Under these assumptions, the characteristic wavelength of sinusoidal wrinkles has a similar expression as eqn (6) except that the plane-strain elastic moduli of the film and the substrate, $\bar{E}_f$ and $\bar{E}_s$, should be replaced by the shear moduli μ_f and μ_s, respectively.[77] It is worth pointing out that other constitutive laws, *e.g.*, Fung and Gent-types,[125,126] can also be used to model the nonlinear responses of biological tissues. Besides skin, similar wrinkling phenomena have been seen in many other layered biological vessels, *e.g.*, those of the pulmonary airway, esophagus, arteries, eustachian tubes, and stomach.[12,32,33,68,127–131] It is believed that wrinkling also plays an important role in the formation of villi and crypts on the inner surface of the small intestine and the colon.[132] In addition, the mechanisms underpinning the wrinkling of film–substrate systems are indicative of morphogenetic events in the stems and fruits of plants.[39,49,50,53] In systems with non-planar geometry, the effect of curvature should be taken into account, especially when the characteristic scales of wrinkles are comparable to the radius of curvature.[46,133] We will detail the morphological instability of non-planar systems in the subsequent sections.

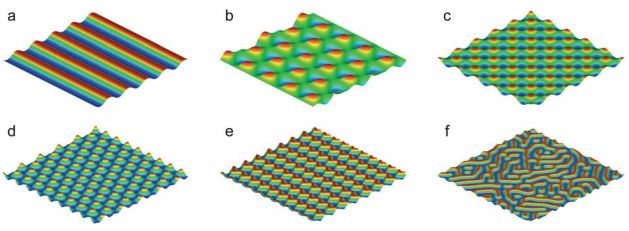

Fig. 9 Wrinkling patterns of stiff films anchored by a compliant substrate: (a) sinusoidal pattern, (b) triangular pattern, (c) checkerboard pattern, (d) hexagonal pattern, (e) herringbone pattern, and (f) labyrinthine pattern.

Let us turn to the swelling of hydrogels with a film–substrate configuration similar to animal skin. The swelling of the film may generate strong compressive stresses and induce wrinkling.[134,135] When the volumetric compressibility of the material is accounted for, the strain energy function in the neo-Hookean hyperelastic constitutive model is written as $W = \mu(\alpha_1^2 + \alpha_2^2 + \alpha_3^2 - 3 - \ln J)/2$, where α_i ($i = 1, 2, 3$) are the principal stretches of the total deformation gradient. In this case, Dervaux and Ben Amar derived the critical wavelength of the sinusoidal wrinkles as[77]

$$\lambda = \frac{2\pi}{6^{1/3}} h \left(\frac{\mu_f}{\mu_s}\right)^{1/3} \tag{7}$$

In comparison with the aforementioned solution under the assumption of volumetric incompressibility, eqn (7) predicts a smaller wavelength. In addition, both eqn (6) and (7) show that the critical wavelength at the onset of wrinkling, derived from the linear stability analysis, depends on the geometry and material properties of the system but not on the compressive strain, as in the conventional theory of buckling.

While the linear stability analysis can predict the wavelength at the initial stage of wrinkling, determination of the wrinkle amplitude and the postbuckling morphological evolution requires nonlinear analysis. During postbuckling, the wavelength will vary with the externally applied compressive strain.[136] Due to its notorious difficulty, most postbuckling analyses have resorted to numerical and experimental approaches while a limited number of exact solutions can be obtained in very simple cases or with simplifications.[36,38,120,121,135,137,138]

Pocivavsek *et al.*[139] reported that due to compression, an elastic film floating on a fluid exhibits a sinusoidal wrinkling instability with a characteristic wavelength. Far beyond the onset of instability, the periodical wrinkling state gives way to a large localized fold, as shown in Fig. 10(a). It has been suggested that such localized folds play a significant role in the functions of the lungs.[141,142] Similar folding phenomena were observed when a floating thin film is lifted by a spherical probe, where the circumferential compression increases as the probe rises.[143] When the water substrate is replaced by an elastic medium, the system shows distinctly different pattern evolution with increasing compression.[140] Further compression above the onset of buckling triggers a secondary bifurcation: one wrinkle grows in amplitude at the expense of its neighbors. This bifurcation creates a period-doubling morphology (Fig. 10(b)). Moreover, a period-quadrupling bifurcation appears under progressive compression (Fig. 10(c)). Li *et al.*[68] numerically reproduced these interesting phenomena by using a pseudo dynamic solution method, as shown in Fig. 10(d) and 10(e). Very recently, Cao and Hutchinson[144] predicted a newly identified mountain ridge mode in the postbuckling of a bilayer system wherein an unstretched

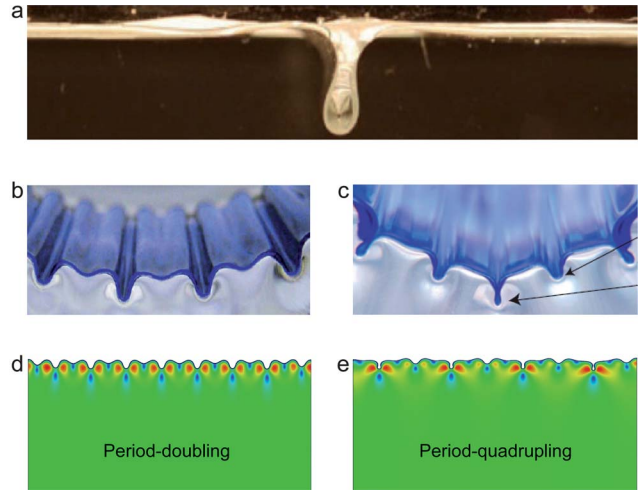

Fig. 10 Morphological evolution during postbuckling: (a) folding of a floating film,[139] (b) period-doubling wrinkling,[140] (c) period-quadrupling wrinkling,[140] (d) FEM results for period-doubling wrinkling, and (e) FEM results for period-doubling wrinkling.[68] Reprinted from ref. 139 and 140 with permission.

film is bonded to a pre-stretched substrate with buckling arising as the stretch in the substrate is relaxed. While the occurrence of this pattern spans a large range of the modulus ratio, say $4 \leq \mu_f/\mu_s \leq 1000$, it depends strongly on the pre-stretching strain of the substrate: only sufficiently large pre-stretch causes mountain ridging. In addition, hierarchical folding can be detected under continuous biaxial-compression: the folds delineate individual domains and each domain is subdivided into smaller ones over multiple generations.[138]

Furthermore, it is worth mentioning that in viscous or viscoelastic materials, wrinkling patterns may evolve with time due to their time-dependent mechanical properties.[145,146] In such systems, the instability characteristics can be determined by integrating the methods of energetics and kinetics.[147] However, investigations on the effects of viscosity on wrinkling pattern evolution are still very limited and deserve much further effort.

5. Soft layers supported by a rigid substrate

In many situations, the constrained growth or swelling of soft materials can be modeled as a system consisting of a soft layer bonded on a rigid substrate. When the soft layer undergoes a volumetric expansion due to water imbibing (swelling) or mass addition (growth), the induced compressive stresses may also render an initially flat film surface unstable, leading to the formation of various surface patterns. For example, Cai *et al.*[75] observed that the swelling of fermenting dough in a bowl is frustrated in the in-plane direction, and when the volumetric expansion reaches a threshold, surface instability occurs, leading to creases on the dough surface, as shown in Fig. 11.[75] This instability, often called creasing, is localized at the free surface of the soft materials and manifests itself by sharp sulci with finite depth (amplitude) and self-contact (Fig. 1(c)),[43,45,75,148–152] somewhat reminiscent of surface cusps arising from the stress-driven surface roughening in heteroepitaxial thin films.[153] The characteristic of creasing instability is quite different from the initial buckling of a stiff film bonded to a compliant substrate, where the entire film is "homogeneously" subjected to deformation coming from the instability.[154] Creases may look like folds, yet they are essentially different. While folds tend to emerge from postbuckling evolution during a wrinkling process, the formation of a crease often undergoes a discontinuous transition from a flat surface to a sharp cusp, bypassing the wrinkling state. Furthermore, while creases are highly sensitive to surface defects and perturbations,[151] folds are relatively stable.[155] Therefore, as two most representative postbuckling processes involving energy localization, creasing and folding have some distinctly different features that deserve further detailed research.

For illustration, we consider an isotropically growing soft layer bonded to a rigid substrate, with the growth tensor expressed as $\mathbf{F}_g = g\mathbf{I}$. For simplicity, the soft layer is assumed to be an incompressible neo-Hookean material. Following a linear stability analysis on an infinitesimal sinusoidal perturbation, the critical growth g_{crit} for the onset of surface instability is determined as $g_{crit}^{2D} = 1.8393$ for the 2D plane-strain case and $g_{crit}^{3D} = 1.5012$ for the 3D biaxial case.[78] It is found that the volumetric changes at the critical buckling state in both 2D and 3D have the same value: $J_G = (g_{crit}^{2D})^2 = (g_{crit}^{3D})^3 = 3.383$. From the solution of $g_{crit}^{2D} = 1.8393$ in the 2D case, one obtains the critical elastic stretch ratio at the occurrence of sinusoidal wrinkling as $\alpha = 1/g_{crit}^{2D} = 54.4\%$. Thereby, the critical compressive Green's elastic strain is $(\alpha^2 - 1)/2 = -35.2\%$ and the nominal strain is $\alpha - 1 = -45.6\%$, which is in accordance with the solution of Biot.[156] However, the wavenumber for the sinusoidal wrinkling pattern is infinite, or in other words, the wrinkling wavelength is undetermined and can be arbitrarily small in the soft layer-rigid substrate system. This surprising result was also predicted by Biot,[156] and he believed that the wavelength at the critical state can be determined by introducing such factors as inhomogeneities and surface irregularities in the material. Ben Amar and Ciarletta[78] argued that the reason why the wavelength cannot be determined lies in the lack of competition between characteristic length scales. Since the gel is represented by a neo-Hookean model having no material length dependence, there is only one scale, *i.e.*, the initial thickness of the layer, serving as the length unit in the whole system. This lack of characteristic length makes it impossible to relate the wavelength of wrinkling to any physical length scale and, consequently, there exists no critical

Fig. 11 Surface creasing of a dough swelling of in a bowl.[75] Reprinted from ref. 75 with permission.

wavelength.[78] Therefore, it is necessary to take into account other physical effects, such as surface tension[78,157] electrostatic force,[158] and strengthening by strain gradients,[151] to regularize the characteristic wavelength to a finite value. In addition to these physical effects, geometrical factors such as the curvature of the substrate can also be utilized to regularize the characteristic wavelength.[33,159]

With the introduction of surface tension γ, the characteristic elastocapillary length $L = \gamma/\mu$ enters the system. Thereafter, the characteristic wavelength is fixed as[78]

$$\lambda = \frac{4\pi H}{\ln(32.246H/L)} \quad (8)$$

where H denotes the thickness of the soft layer. Eqn (8) demonstrates that the wavelength is of order of the initial thickness, and surface tension plays the role of setting and amplifying the wavelength. Clearly, the wavelength has a nonlinear dependence on the thickness H. Eqn (8) works for the constrained growth of the soft layer. When it comes to the case of volumetric change incurred by water imbibing, the wavelength is modified as[77]

$$\lambda = \frac{4\pi H}{\ln(44.953H/L)} \quad (9)$$

Although the critical wavelength can be regularized by introducing another length scale, as given in eqn (8) and (9), the sinusoidal wrinkles remain highly unstable and lead to crease formation soon after the onset of wrinkling.[151] In the case of a soft layer constrained by a rigid substrate,[45,160] therefore, discretized creases occur instead of well-developed sinusoidal wrinkles. In this sense, creasing can be regarded as a collapsed state of wrinkling.[151]

6. Cylinders and tubes

Long cylinders or tubes typically exhibit two buckling modes, namely surface buckling with the central axis remaining straight and global buckling with a wavy axis like an Euler bar or with a curling axis. In such systems, 2D or 3D elasticity should be utilized to uncover surface instability while beam models are usually adopted to deal with global buckling. In some situations, the two modes may take place simultaneously, as in the case of morphogenesis in the small intestine of human.

6.1. Surface buckling

Many one-dimensional soft materials such as fibers, rods, wires, cylinders and tubes have a relatively stiff skin. An example is electrospun polymer fibers.[133] Such core–shell structured materials hold promise for important applications in, for instance, drug delivery, enzyme supports, biosensors and functionalized coatings.[161–163]

As the circumferential compressive stress in the shell reaches a critical value, surface buckling becomes energetically favored over uniform deformation. The characteristic wavelength is selected to minimize the total energy of the system.[133,164] Based on the idea of surface buckling, Yin *et al.*[164] suggested a novel approach for fabricating microcomponents with designed surface structures, *e.g.*, microgears. Their analysis demonstrated that cylindrical core–shell fibers may buckle into sinusoidal morphologies with a designed wavelength dictated by different geometrical and material parameters.[165] Recently, Cao *et al.*[166] found that when the swelling of the shell with thickness H or the shrinkage of the core with radius A reaches a larger threshold, the pattern bifurcates again and a wrinkle-to-fold transition occurs, rendering a period-doubling surface topography, as shown in Fig. 12. This wrinkle-to-fold transition is also a process of increasing stress concentration. As can be seen from the right inset in Fig. 12, stress distribution is localized in narrow ridges of the patterns. The FvK number $\eta \propto (A/H)^2$, defined in the theory of elastic plates and shells,[167] can be used to characterize the relative importance of tensile and bending rigidities. Since η is large at small shell thickness, the deformation of the shell favors pure bending almost everywhere except at the folding ridges where the energetically expensive stretching is localized. Therefore, the competition between the stretching/shearing-dominated deformations in the core and the bending-dominated deformations in the shell leads to the wrinkle-to-fold transition. Although the emergence of the wrinkle-to-fold transition requires a large modulus ratio, the second critical shrinkage magnitude is almost independent of the modulus ratio between the shell and the core.[166]

In addition to the artificial structures, surface wrinkling may also occur in tubular organs of animals such as the esophagus, pulmonary airway, eustachian tube, gastrointestinal tract and many other animal lumens (see Fig. 13(a) for an image of bovine esophagus).[12,32,128,168,169] These organs normally consist of a muscular, a submucosal, and a mucosal layer (Fig. 13(a)). The muscular layer is usually much stiffer than the submucosal layer. The submucosal layer consists of loosely connective tissue on the luminal side of the muscle. The mucosal layer includes the lamina propria or subepithelial collagen layer, the basement membrane, and the epithelium. The ratio between the elastic moduli of mucosa and submucosa can vary in a broad range, *e.g.*, 1–314.[127] The modulus of the combined mucosa–submucosa layer is in the range of 3–24 kPa for the pulmonary airway of rabbits[170] and about 0.5 kPa for porcine esophagus.[12] Most previous studies believed that wrinkling at the inner surface of these tubular organs arises from smooth muscle contraction or external mechanical loads.[12,32,127,128] However, an alternative explanation is that the wrinkling/folding occurs as a consequence of constrained tissue growth. Recently, both

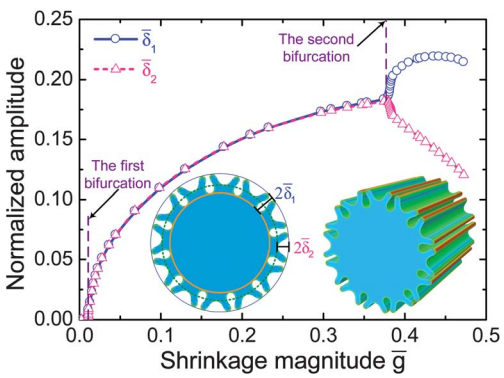

Fig. 12 Wrinkle-to-fold transition occurring in a core–shell cylinder.[166]

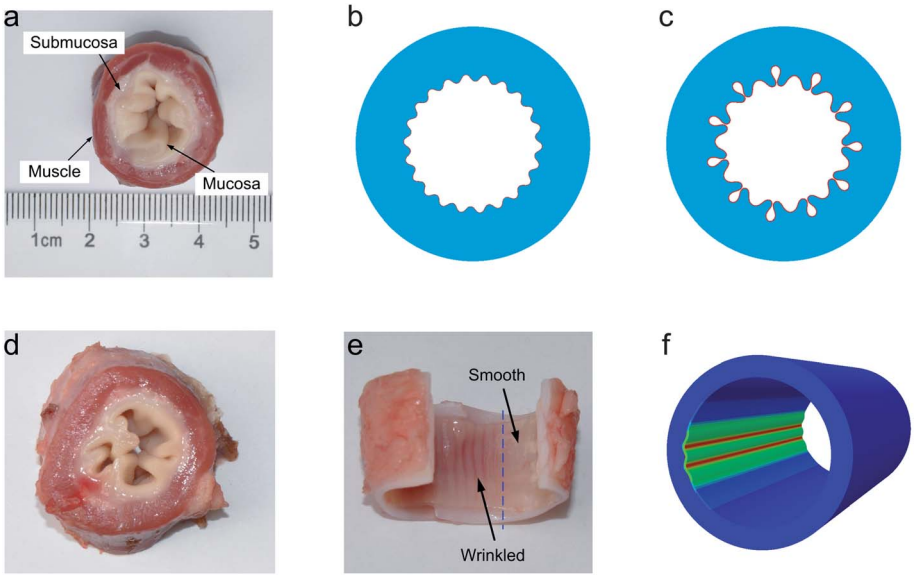

Fig. 13 Wrinkling in tubular organs: (a) a ring cut from bovine esophagus, (b) sinusoidal wrinkling induced by mucosal growth, (c) period-doubling pattern induced by large growth, (d) period-doubling pattern in bovine esophagus, (e) local wrinkling in porcine airway and (f) numerical simulation for local wrinkling.[68]

single-layer and bilayer models have been proposed to elucidate the growth-driving mechanisms underpinning surface wrinkling observed in these soft tissues (Fig. 13(b)).[33,68,159,171,172] These studies have potential applications in clinical diagnose of some diseases such as inflammation, edema, lymphoma, asthma, and enterogastritis. Abnormal growth and alteration of wrinkling patterns in mucosa are important clinical signs and symptoms of diseases.[32,173,174] For instance, clinical observations found that asthmatic airways exhibit folds deeper than normal.[128,169] In addition, wrinkling on the inner surface of a tube offers the prospect of generating corrugated surfaces on polymeric gels with adjustable roughness in a confined space, which can be used to control actively the adhesive and frictional property for fluid transport.[47,75] Experimental observations and numerical simulations provided evidence that similar period-doubling folds can appear in growing tubular biological tissues (Fig. 13(c) and 13(d)).[68,142] In addition, the volumetric growth of soft tissues is not always homogeneous and can be highly localized or inhomogeneous for various reasons.[175] Biological tissues may undergo instabilities as a result of these growth forms.[68] For example, a porcine airway with local wrinkling is shown in Fig. 13(e), which has been reproduced by Li *et al.*[68] using FEM simulations (Fig. 13(f)).

Due to the similarities in the wrinkling characteristics, here we also discuss the instability in some systems satisfying the plane-strain or plane-stress (with the longitudinal dimension comparable to or even shorter than the cross-sectional sizes, *e.g.*, a disk) conditions. Following the sinusoidal wrinkling on the surface of a disk consisting of a soft shell on a hard core (Fig. 14(a)), the surface instability often manifests itself by creasing (Fig. 14(b)).[34] For the wrinkle-to-fold transition occurring in a soft core with a hard shell, every two neighboring crests would merge into a single and large bump, creating a period-doubling topography. Besides, a growing soft layer resting on the wall of a stiff tube may also trigger a creasing instability.[40]

A fiber growing in both the cross section and the longitudinal directions would develop a 3D wrinkling pattern. If the skins of the cylindrical tissues consist of fibrous layers with a preferred orientation, or the growth of the structures is anisotropic, a torsional buckling can be triggered, forming helical patterns (Fig. 14(c)).[176] Interestingly, multiple bifurcations may take place with increasing growth, leading to morphological transitions from trench to hexagon and finally to labyrinth patterns (Fig. 14(c)).[177] It should be pointed out that the axial (Fig. 14(d)) or combined wrinkling in both circumferential and axial directions may be energetically favored for cylinder or tubular tissues growing along the longitudinal direction.[65,131,132,178]

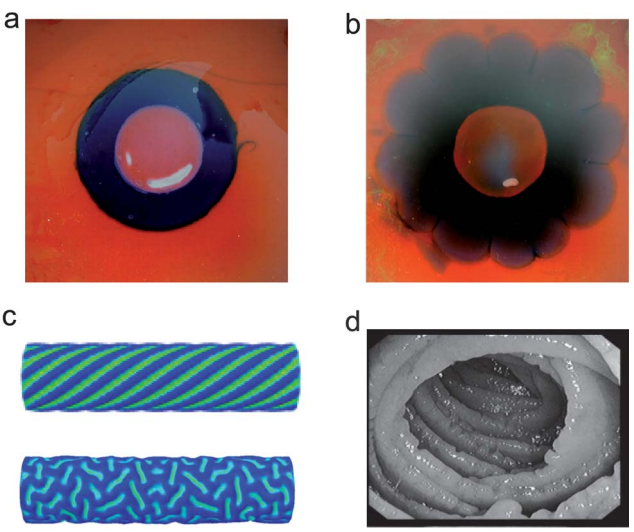

Fig. 14 Swelling of a soft layer bonded to a hard core: (a) the initial state before swelling and (b) creasing state.[77] (c) Torsional buckling induced by anisotropic growth in a core–shell cylinder.[177] (d) Axial wrinkling in a jejunum.[179] Reprinted from ref. 77 and 179 with permission.

6.2. Global buckling

As mentioned above, many growing cylindrical structures such as plant stems, arteries and small intestines may also undergo a global Euler buckling to lower the total potential energy of the system.[65,180–182] For example, tortuosity or kinking caused by the global instability often occurs in human internal carotid arteries or iliac arteries with significant clinical complications,[183] and the buckling of the internal carotid artery can engender stroke, vertigo, syncopes, blackout, persistent tinnitus, and other cerebrovascular diseases.[184–186]

It is well known that a clamped–clamped beam may buckle into a half sinusoidal wave while multiple sinusoidal waves are preferred when it is bonded on a soft substrate.[24,187–189] However, tubular organs (*e.g.*, arteries, veins and guts) are often supported by their surrounding tissues *in vivo*. Therefore, the Euler buckling model for fibers or tubes may not give the best prediction for the morphogenesis in organ development. More realistic models which take into account the effects of elastic supports have been proposed.[190] Most recently, Savin *et al.*[31] suggested a biomechanical model to unravel the gut looping morphogenesis caused by the mismatch in growth between the gut tube and the anchoring dorsal mesenteric sheet. A gut forms as a simple linear tube of circular cross-section running down the midline of the embryo, and grows at a greater rate than the surrounding mesenteric sheet, eventually becoming significantly longer than the trunk. Owing to the constraints from the mesenteric sheet and the capacity of the body cavity, the gut is first forced into a wavy configuration with moderate growth and then to loop around with greater growth, as shown in Fig. 15(a) and 15(b). This wrinkling phenomenon can be reproduced by using a rubber model (Fig. 15(c) and 15(d)), where the effect of growth is uncovered. The wavelength λ of the first stage and the radius R_{loop} of the loop forming in the consequent stage can be expressed as[31]

$$\lambda \propto \left(\frac{E_{\text{gut}} I_{\text{gut}}}{E_{\text{sheet}} h}\right)^{1/3}, \quad R_{\text{loop}} \propto \left(\frac{E_{\text{gut}} I_{\text{gut}}}{E_{\text{sheet}} h \varepsilon_0^2}\right)^{1/3} \tag{10}$$

where E_{gut} and E_{sheet} are the Young's moduli of the gut and the mesenteric sheet, respectively, I_{gut} denotes the cross-sectional moment of inertia of the gut tube, ε_0 is the elastic strain and h is the thickness of the mesenteric sheet.

Besides the applications in morphogenesis of soft tissues, buckling metrology has also been proposed to estimate the mechanical properties of cylinders, *e.g.*, plant stems.[65] Because beam models are usually employed in the global buckling analysis, the buckling metrology can also be applied to other geometrical configurations, for example, measuring the elastic modulus of nanowires with various shapes by wrinkling them on a compliant substrate.[24]

7. Spheres and cavities

Much experimental effort has been directed toward the synthesis of core–shell or multi-layer structured soft particles,[71,191,192] with promising applications in drug delivery, enzyme supports and biosensors. Recently, engineering of the geometrical characteristics of surface texture has gained recognition for their potential to alter the properties of particles, especially in the biological and

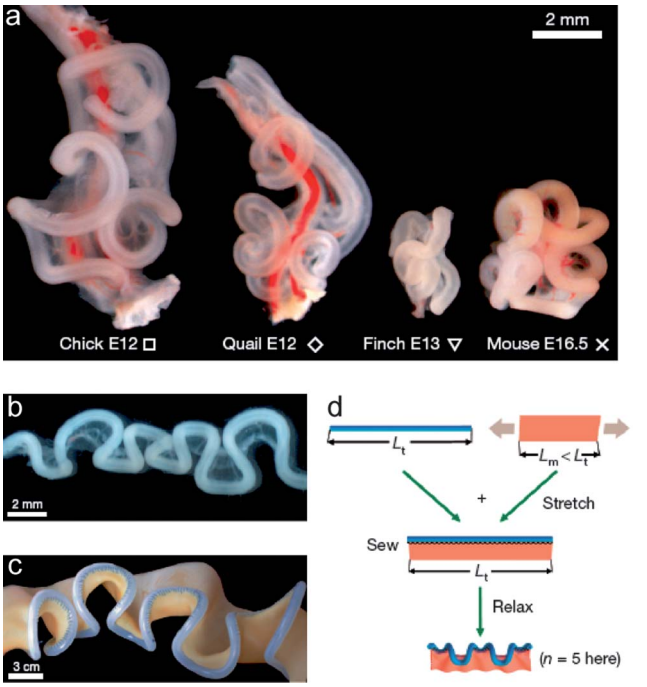

Fig. 15 Wrinkling of guts in animal: (a) gut looping patterns in a chick, quail, finch and mouse, (b) aligned gut of a chick, (c) composite rubber model, and (d) theoretical model.[31] Reprinted from ref. 31 with permission.

biomedical fields. However, the controllable fabrication of morphology on soft particles often requires complicated procedures that change their originally smooth appearance.[193] In recent years, it has been increasingly recognized that the differential swelling/shrinkage originating from physical and chemical mechanisms in core–shell structures can trigger various morphological instabilities, providing a novel and facile way for surface patterning of particles.[39,194]

Moreover, many fruits or plants also have core–shell structures, *e.g.*, Korean melon, ridged gourd, small pumpkin, and acorn squash, which lead to various surface patterns. The intrinsic mechanisms underlying the morphogenesis of a growing fruit, according to Charles Darwin, could "drive the sanest man mad" and remain far from being uncovered. Yin *et al.*[49,50] argued that mechanical buckling incurred by the mismatch in growth between the shell and the core may have important implications on the formation of these patterns. Based on the theory of a thin elastic shell, they discussed the stability of various spheroidal structures with different equatorial and polar radii, and related the characteristic patterns to those observed on the surfaces of fruits. Besides, dehydration of pollen grains and green fruits such as peas and grapes indeed gives rise to mechanical buckling and subsequent formation of various surface patterns.[39,195]

Recently, Li *et al.*[196] carried out theoretical analysis and nonlinear FEM simulations to elucidate the wrinkling on a soft neo-Hookean core–shell sphere induced by shrinkage of the core. Initially, the sphere shrinks isotropically (Fig. 16(a)). As the shrinkage reaches a critical value, the sphere suddenly bifurcates into a periodic dimple structure to release circumferential compression in the shell (Fig. 16(b)). With further shrinking, a pattern consisting of regular pentagons and hexagons

characterizes the surface of the sphere, as shown in Fig. 16(c). Such a pattern is reminiscent of the structure of the buckyball (Fig. 16(k) and 16(i)). As the shrinkage increases further, a second bifurcation (wrinkle-to-fold) takes place and the buckyball pattern from the first bifurcation breaks into fold-like structures: some polygons narrow into troughs, while others merge with their neighbors (Fig. 16(d)). In comparison with the buckyball pattern, the folding patterns can release more elastic strain energy at this stage. Finally, the spherical surface evolves toward a labyrinthine pattern (Fig. 16(e)), corresponding to the further localization of elastic strain energy. This evolution process has been confirmed by the dehydration of green peas, as shown in Fig. 16(f)–(j). To some extent, this furrowed pattern resembles the topography of brain folds (Fig. 16(m)).[197]

The morphological evolution can be understood from an energetic view. For a core–shell sphere with core radius A and shell thickness H, as show in Fig. 17(a), the normalized total energy $\bar{U}$ of the system increases as a function of the shrinking factor $\bar{g}$ of the core, where $U = \int_{\Omega} J[W - p(\det \mathbf{A} - 1)]\mathrm{d}\Omega$, p is a Lagrangian multiplier, Ω the initial volume occupied by the sphere and $\bar{U} = U/(\mu_c A^3)$, μ_s and μ_c denote the shear moduli of the shell and the core, respectively. The energy variation from FEM simulations is in good agreement with the theoretical solution prior to the onset of buckling (region I). When the shrinkage exceeds a critical value, $\bar{g}_{crit}$, the spherical surface buckles and the system enters region II as a consequence of energy minimization. With further shrinking, a buckyball pattern characterizes the surface of the sphere. As the shrinkage increases further, the buckyball pattern is not energetically optimal any more. To reduce the total energy, a second bifurcation may take place and the system enters region III. The buckyball pattern from the first bifurcation breaks into fold-like structures. In

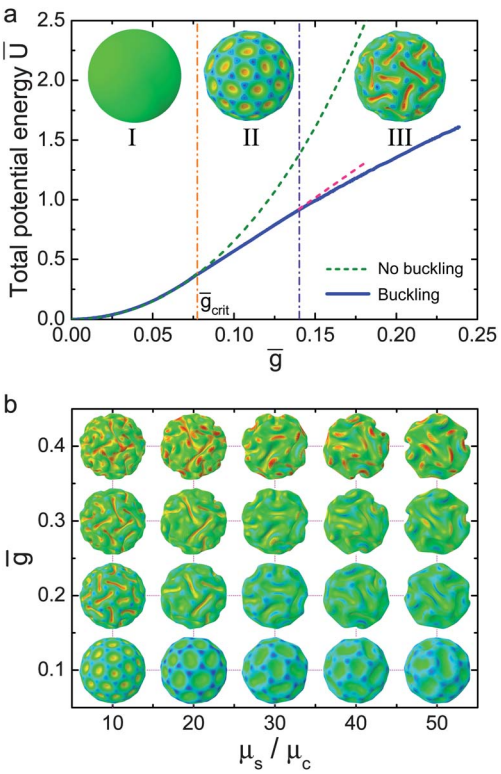

Fig. 17 (a) Energetic mechanism underpinning the wrinkle-to-fold transition, where $\mu_s/\mu_c = 10$. (b) Evolution of the surface morphologies of spheres with different values of μ_s/μ_c. In this figure, the core radius $A = 100$ and the shell thickness $H = 4$.[196]

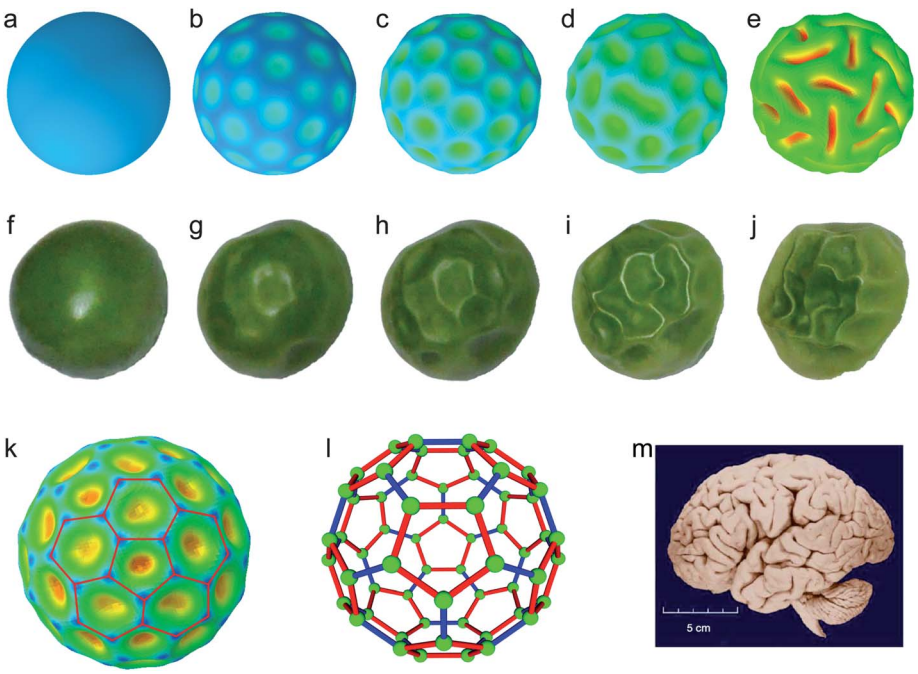

Fig. 16 Wrinkling of soft core–shell spheres. (a)–(e) Displacement on the spherical surface caused by shrinkage of the core and (f)–(j) experimental observations in dehydration of a green pea. From left to right, the time interval is one hour. (k) Buckyball-like pattern. (l) Buckyball.[196] (m) Human brain.[197] Reprinted from ref. 197 with permission.

addition, the modulus ratio between the shell and the core can be used to modulate the topography: thick folding occurs when μ_s/μ_c is large and *vice versa* (Fig. 17(b)).

The morphological instability in core–shell soft structures that incorporate growth may also have important implications on tumor development and invasion. Many types of mammalian cells can aggregate into multicellular tumors with spherical shapes (*e.g.*, cervical squamous cell carcinoma, see Fig. 18(a)).[198] The early development stages (avascular phase) of solid tumors are apparently regulated by the diffusion of nutrients within the extracellular matrix. However, the consumption of the nutrients means that their concentration must decrease toward the center of the tumor. When the available nutrients at the center fall below the critical level to sustain cell life, a core–shell structure develops with a central necrotic core surrounded by layers of distinct levels of cellular activity.[199] A tumor, therefore, consists of an inner necrotic core, an intermediate region with quiescent cells, and the outmost rim with actively proliferating cells (Fig. 18(b)).[78,198,200] Such an avascular tumor under development can be modeled as a growing shell enclosing a core of non-grown cells. The growth confined at the periphery of tumors can not only alter the size of the tumors but also elicit residual stresses, which may destabilize the system, engendering multiple symmetry breaking processes and varied topographies. It is believed that this surface instability, breaking a uniform and compact tumor front into wavy and irregular morphologies, as observed in experiments, dramatically correlates with increased tumor aggressiveness (Fig. 18(c)).[201–203] The mechanical stability analysis suggests that increasing the thickness and reducing the stiffness of a proliferative cellular layer can inhibit the invasion of the tumor. Besides, growth beyond the critical instability renders labyrinthine patterns consisting of ridges and troughs, which sheds light on the intricate pattern on the tumor surface. Although many biochemical processes are involved in the onset of invasion of a solid tumor, mechanics and chemistry should be considered on an equal footing to describe accurately the evolution of tumors.

In systems with negative surface curvature (*i.e.*, cavities), constrained swelling or growth of soft layer will also cause surface buckling and pattern transition. For example, as the mucosal layer grows in the stomach of animals, mechanical buckling is observable due to the constraints of the gastric wall.[129] The surface patterns depend on the elastic modulus and thickness of the mucosa, as well as the radius of curvature of the cavity. A slight increase in the thickness of a thin mucosa may incur significant reduction of surface wrinkles. These pattern changes may be closely related to certain mucosal diseases. For instance, mucosal wrinkles are found to enlarge and thicken in the stomach of patients with eosinophilic gastroenteritis.[204]

8. Vesicles and capsules with or without internal pressure

Soft particles with a hollow interior are often referred to as vesicles or capsules. They are particularly interesting not only for applications in drug carrier, catalysis, and biotechnology, but also are vital for serving as the crust for cells and virus.[205,206] For example, viral capsids, the nanometer-sized protein shells of viruses, are composed of a two-dimensional protein assembly, which serve to contain and protect viral genome molecules.[207] As experimentally observed, both macroscopic and microscopic capsules can buckle and even collapse under external pressure or evaporation of solvent.[208,209] Buckling of vesicles or capsules may pose limits to their engineering applications but also have important implications for the morphology of cells and virus. For example, it has been conjectured that the shapes of spherical viruses with icosahedral symmetry (Fig. 19(a)) are closely associated with their morphological instability.[167,210] Understanding the buckling mechanisms of capsules is helpful for probing their structures and mechanical properties and for gaining new insights into the etiology of relevant diseases.

Lidmar *et al.*[167] argued that the faceting of large viruses is caused by a buckling transition associated with twelve isolated points of five-fold symmetry. The singularity at these points was regarded as a disclination in an otherwise six-coordinated medium. They demonstrated that the faceted shape of viruses depends only on the dimensionless FvK number, $\eta = Y\bar{R}^2/D$, where Y is the 2D Young's modulus of the protein shell, $\bar{R}$ the mean virus radius, and D the bending rigidity. The critical characteristics were determined by considering the competition between the stretching and bending elastic energies of the closed shell. More recently, the instability characteristics and morphogenesis of spherical colloid capsules or viral capsids with non-icosahedral symmetries, *e.g.*, spherocylindrical and conical shells,[211] have been examined with or without volumetric constraint (Fig. 19(b)–(d)).[212–214] These studies showed that the FvK number plays a significant role in the wrinkling of capsules.

To characterize the mechanical properties of a capsule, a point force is often applied on its surface. When the force reaches a threshold, the capsule will buckle and a depression will form. From the geometry of the sunken region, the elastic parameters of the capsule can be determined by an inverse

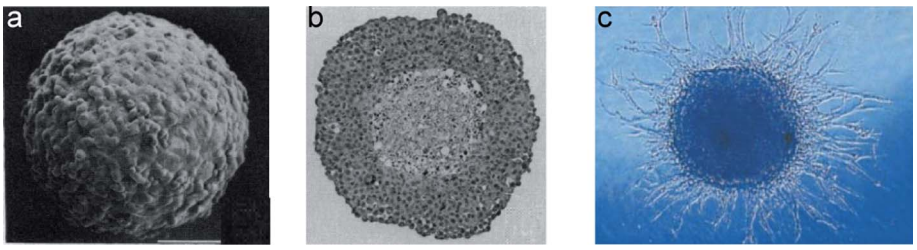

Fig. 18 Solid tumors: (a) scanning electron micrograph of human cervical squamous cell carcinoma spheroid with a diameter about 300 μm and (b) histological section through the center of a solid tumor similar to that shown in (a).[200] (c) Invasion of a spherical solid tumor *in vitro*.[201] Reprinted from ref. 200 and 201 with permission.

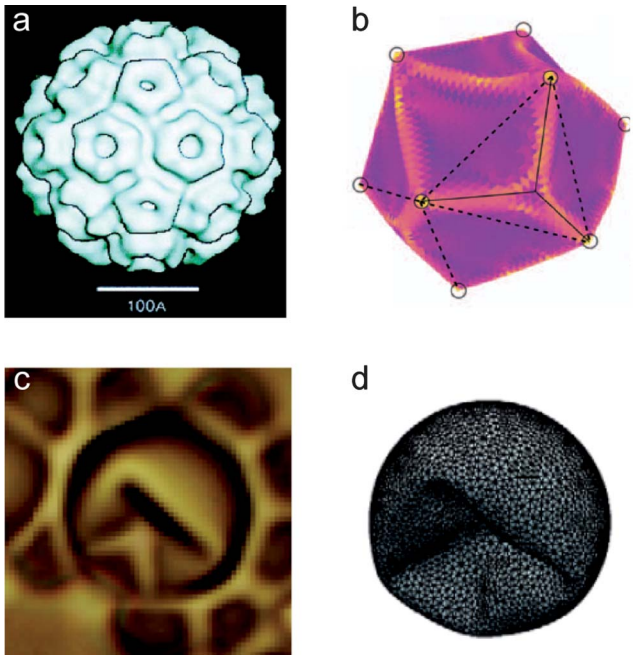

Fig. 19 (a) Cryo-TEM (transmission electron microscopy) reconstruction of the cowpea chlorotic mottle virus.[210] (b) Numerical simulation of the buckling of an icosadeltahedral capsule under external pressure.[213] (c) Transmission optical microscopy of a colloidal capsule with local buckling due to the evaporation in inner solution, and (d) the simulation results corresponding to (c).[214] Reprinted from ref. 210, 213 and 214 with permission.

analysis.[209,215] Using the theory of an elastic thin shell, Vella *et al.*[216] showed that during indentation, the shape of the sunken region is not only contingent on the material properties of the capsule but also on the internal pressure, P. If the shell is unpressurized, a regular triangular structure occurs, as predicted previously.[217] However, increasing the internal pressure will lead to an increase in the number of wrinkles in the annular depression region, as shown in Fig. 20. As the indentation deepens, the size of this annular region increases but the wavenumber n remains constant. For an elastic shell of natural radius R, thickness h, and Young's modulus E, one can define a dimensionless bending stiffness ξ by[216]

$$\xi \propto \frac{P}{E}\left(\frac{R}{h}\right)^2 \tag{11}$$

When $\xi \leq 1$, the depression is expected to have a triangular structure, that is, $n = 3$. When $\xi \gg 1$, the wavenumber scales as $n \propto \xi^{1/2}$. This reveals that one can estimate the elastic modulus of a capsule by counting the number of wrinkles arising from the point indentation.

The above studies provide clues for developing new methods to measure the mechanical properties of capsules, cell membranes, and some other biological structures. In addition, the morphological instability and evolution of capsules are closely associated with the topographical development of cells and virus. Systematic theoretical and experimental investigations on this issue will be of great interest.

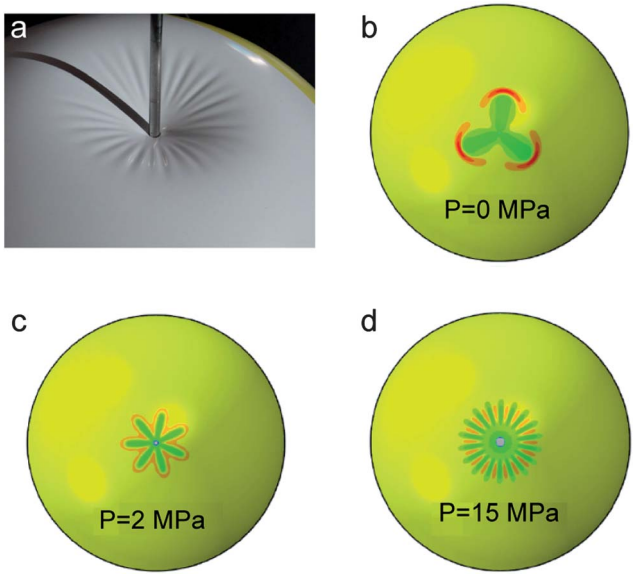

Fig. 20 (a) Wrinkling of a beach ball under point indentation. (b)–(d) The transition from polygonal localizations to wrinkles with increasing internal pressure, where the wavenumbers are 3, 7, and 18, respectively.[216] Reprinted from ref. 216 with permission.

9. Surface instability driven by long-range interactions

Besides the above-described mechanisms that may cause morphological instability, soft materials can also be destabilized by long-range interactions such as van der Waals forces, electric double-layer forces and electrostatic forces, which are normally negligible for macroscopic structures of hard materials. For instance, when a soft thin film bonded to a rigid substrate is approached by a rigid indenter, the film may wrinkle due to its van der Waals interaction with the indenter (Fig. 21(a)).[5,7,8,218,219] This morphological instability occurs due to a competition between the combination of elastic and surface energies, which tend to stabilize the system, and the interaction energy, which acts as the main destabilizing force.[8] When the film thickness is reduced to less than 1 μm, the relationship between the wavelength and the film thickness becomes nonlinear due to the enhanced contribution of surface energy. Besides, the compressibility of the film, which is manifested through Poisson's ratio v, plays a significant role in the surface instability. For $v \leq 1/4$, the film undergoes a stable and homogeneous deformation insensitive to surface perturbations. For $v > 1/4$, however, the film prefers surface undulation to lower the potential energy of the system when the van der Waals interaction force with the indenter reaches a critical value.[7,218] This indicates that highly compressible films tend to deform uniformly.

It is noticed that the buckling-induced surface patterns depend strongly on the mechanism that triggers the instability. A soft layer resting on a rigid substrate will buckle into a stable sinusoidal wrinkling patter when subjected to the van der Waals interaction force. In contrast, under in-plane compression the sinusoidal pattern is unstable and a wrinkle-to-crease transition occurs soon after the occurrence of buckling. In addition, the wrinkling behavior of a thin elastic film is different from

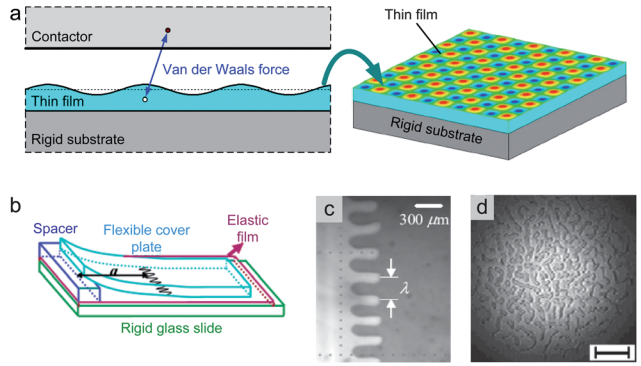

Fig. 21 Surface wrinkling induced by long-range interaction forces: (a) interaction between a thin film and a contacting solid; (b) peeling of adhesive;[233] (c) finger instability[238] and (d) worm-like instability.[233] Reprinted from ref. 233 and 238 with permission.

a viscous liquid film.[220–223] If the surface energy of the film is negligible, the instability-induced pattern wavelength in the former case is proportional to the film thickness but independent of the nature of the interaction force normal to the film surface, while in the latter case, the wavelength and pattern characteristics depend strongly on the nature and magnitude of the external stimuli.

Besides the external stimuli, such interactions as van der Waals forces and electrostatic forces within the system can also trigger surface bifurcation, commonly referred to as spontaneous instability.[224–226] For a planar thin elastic film bonded on a rigid substrate, the characteristic wrinkling wavelength of the spontaneous instability is contingent on the film thickness *via* an exponential relation with power index in the range of 0.75–1.0, depending on the ratio between the surface energy and shear modulus of the film.[225] In addition, it is emphasized that the surface curvature of the substrate plays a significant role in the wrinkling behavior. To uncover the effect of surface curvature, Li *et al.*[226] presented a generic method for analyzing the surface stability of a thin film interacting with the substrate. In particular, they discussed several important geometric configurations with either a positive or negative mean curvature. The above results on the surface instability of soft films under different driving forces may find important applications in a number of fields including soft lithography. It is also indicated that one may fabricate nanopatterns or enhance the surface stability of soft thin films by modulating the mechanical properties of the films and/or geometrical properties such as film thickness and substrate curvature.

Recently, wrinkling phenomena in several other complex systems have also been studied, *e.g.* a soft bilayer, mutually attracting films, and a thin film on a patterned or slipping substrate.[227–232] For instance, when a thin elastic film is peeled from a rigid flat surface, its surface loses its planarity and subsequently evolves into a fingering shape (Fig. 21(b) and 21(c)) or a worm-like pattern (Fig. 21(d)) with a fairly regular spacing.[233–237] The wavelength of this instability varies linearly only with the thickness but is independent of other properties of the film. However, different behavior is observed when the peeling takes place between two soft elastic solids. In this case, the wavelength becomes a nonlinear function that depends not only on the thicknesses but also on the elastic properties of the two materials.[238] This issue is of fundamental importance for understanding the effects of elastic instability on the interfacial properties such as friction, adhesion, and failure.

10. Conclusions

This review has been aimed to provide an illustrative glance at the rich phenomenon of morphological instability and surface wrinkling in soft materials. The wrinkling behavior depends strongly on the geometric configuration of the system, and we have discussed the wrinkling patterns and morphological evolution in some representative configurations, including thin films, sheets, fibers, particles, tubes, cavities, and capsules, with particular attention on the surface instability induced by volumetric growth/shrinkage. Some of the recent advances in the 2D and 3D modeling of critical buckling and postbuckling have also been briefly discussed.

Although remarkable progress has been made in recent years on the modeling of morphological instability in soft matter, there remain heaps of significant and interesting problems that deserve further experimental and theoretical investigation. First of all, advances in theoretical modeling in this field are hindered by a number of mechanical and mathematical complexities. For example, the surface instability of soft materials usually involves both strong geometrical and material nonlinearities, making the theoretical analysis difficult. The morphological evolution beyond the critical state is incredibly complicated, especially in the case of 3D surface instability on curved surfaces, and the conventional methods of buckling have difficulties in predicting surface patterns and their evolution. The postbuckling evolution of surface wrinkling often involves large deformation, nonlinear constitutive relations, multiple symmetry-breakings, loading path-dependence, stress singularity, and other complexities. In addition, as to the morphogenesis of living tissues and organs, a number of chemical and biological mechanisms, which couple with the mechanical factors, may contribute to the wrinkling behavior but so far little progress has been made in this direction. Systematic investigations on the influence of these mechanisms would be of interest not only for understanding the morphological evolution of living tissues but also for the diagnosis and treatment of some diseases. Therefore, it is of significance to develop more effective methods for studying the buckling and postbuckling behavior of soft materials taking into account the effects of biological–chemical–mechanical coupling, 3D geometry, and other influential factors. Finally, it is worth mentioning that much effort has been directed toward exploring the applications of buckling-based techniques for the surface patterning of materials (*e.g.*, soft lithography and imprinting), mechanical and physical measurements of material properties (*e.g.*, Young's modulus and Poisson's ratio), medical and biological applications (*e.g.*, prevention of skin wrinkles), most of which have not been included in this review.

Acknowledgements

Support from the National Natural Science Foundation of China (grant no. 10972121, 10732050, and 11172155), Tsinghua University (2009THZ02122), the 973 Program of MOST

(2010CB631005 and 2012CB934101), and the SRFDP Program of MOE (20090002110047) is gratefully acknowledged. We also wish to thank Professors H. Y. Liang and H. M. Xie for their helpful suggestions.

References

1 S. C. Cowin, *Annu. Rev. Biomed. Eng.*, 2004, **6**, 77–107.
2 J. Kopecek, *Biomaterials*, 2007, **28**, 5185–5192.
3 J. Genzer and J. Groenewold, *Soft Matter*, 2006, **2**, 310–323.
4 L. He and L. Qiao, *Europhys. Lett.*, 2007, **80**, 14003.
5 W. Monch and S. Herminghaus, *Europhys. Lett.*, 2001, **53**, 525–531.
6 K. Li and L. He, *Int. J. Solids Struct.*, 2010, **47**, 2784–2789.
7 S. Q. Huang, Q. Y. Li, X. Q. Feng and S. W. Yu, *Mech. Mater.*, 2006, **38**, 88–99.
8 V. Shenoy and A. Sharma, *Phys. Rev. Lett.*, 2001, **86**, 119–122.
9 W. Hong, X. Zhao, J. Zhou and Z. Suo, *J. Mech. Phys. Solids*, 2008, **56**, 1779–1793.
10 I. Tokarev and S. Minko, *Soft Matter*, 2009, **5**, 511–524.
11 B. Li, X. Q. Feng, Y. Li and G. F. Wang, *Appl. Phys. Lett.*, 2009, **95**, 021903.
12 W. Yang, T. Fung, K. Chian and C. Chong, *J. Biomech.*, 2007, **40**, 481–490.
13 M. Guvendiren, S. Yang and J. A. Burdick, *Adv. Funct. Mater.*, 2009, **19**, 3038–3045.
14 S. Singamaneni, M. E. McConney and V. V. Tsukruk, *Adv. Mater.*, 2010, **22**, 1263–1268.
15 P. J. Yoo, K. Y. Suh, S. Y. Park and H. H. Lee, *Adv. Mater.*, 2002, **14**, 1383–1387.
16 E. P. Chan and A. J. Crosby, *Adv. Mater.*, 2006, **18**, 3238–3242.
17 D. Chandra, S. Yang and P. C. Lin, *Appl. Phys. Lett.*, 2007, **91**, 251912.
18 H. Mei, R. Huang, J. Y. Chung, C. M. Stafford and H. H. Yu, *Appl. Phys. Lett.*, 2007, **90**, 151902.
19 D. H. Kim and J. A. Rogers, *Adv. Mater.*, 2008, **20**, 4887–4892.
20 A. J. Baca, J. H. Ahn, Y. Sun, M. A. Meitl, E. Menard, H. S. Kim, W. M. Choi, D. H. Kim, Y. Huang and J. A. Rogers, *Angew. Chem., Int. Ed.*, 2008, **47**, 5524–5542.
21 W. M. Choi, J. Song, D. Y. Khang, H. Jiang, Y. Y. Huang and J. A. Rogers, *Nano Lett.*, 2007, **7**, 1655–1663.
22 J. Y. Chung, A. J. Nolte and C. M. Stafford, *Adv. Mater.*, 2011, **23**, 349–368.
23 B. Li, S. Q. Huang and X. Q. Feng, *Arch. Appl. Mech.*, 2010, **80**, 175–188.
24 Y. P. Cao, X. P. Zheng, B. Li and X. Q. Feng, *Scr. Mater.*, 2009, **61**, 1044–1047.
25 C. M. Stafford, C. Harrison, K. L. Beers, A. Karim, E. J. Amis, M. R. VanLandingham, H. C. Kim, W. Volksen, R. D. Miller and E. E. Simonyi, *Nat. Mater.*, 2004, **3**, 545–550.
26 E. Sharon, M. Marder and H. L. Swinney, *Am. Sci.*, 2004, **92**, 254–261.
27 M. Ben Amar and A. Goriely, *J. Mech. Phys. Solids*, 2005, **53**, 2284–2319.
28 H. Liang and L. Mahadevan, *Proc. Natl. Acad. Sci. U. S. A.*, 2009, **106**, 22049–22054.
29 D. W. Thompson, *On Growth and Form*, Cambridge University Press, 1942.
30 A. Boudaoud, *Trends Plant Sci.*, 2010, **15**, 353–360.
31 T. Savin, N. A. Kurpios, A. E. Shyer, P. Florescu, H. Liang, L. Mahadevan and C. J. Tabin, *Nature*, 2011, **476**, 57–62.
32 B. R. Wiggs, C. A. Hrousis, J. M. Drazen and R. D. Kamm, *J. Appl. Physiol.*, 1997, **83**, 1814–1821.
33 B. Li, Y. P. Cao and X. Q. Feng, *J. Biomech.*, 2011, **44**, 182–188.
34 J. Dervaux, Y. Couder, M. A. Guedeau-Boudeville and M. B. Amar, *Phys. Rev. Lett.*, 2011, **107**, 018103.
35 A. Schweikart and A. Fery, *Microchim. Acta*, 2009, **165**, 249–263.
36 S. Cai, D. Breid, A. J. Crosby, Z. Suo and J. W. Hutchinson, *J. Mech. Phys. Solids*, 2011, **59**, 1094–1114.
37 Z. Huang, W. Hong and Z. Suo, *J. Mech. Phys. Solids*, 2005, **53**, 2101–2118.
38 B. Audoly and A. Boudaoud, *J. Mech. Phys. Solids*, 2008, **56**, 2401–2421.
39 E. Cerda and L. Mahadevan, *Phys. Rev. Lett.*, 2003, **90**, 074302.
40 L. Jin, S. Cai and Z. Suo, *Europhys. Lett.*, 2011, **95**, 64002.
41 J.-Y. Sun, S. Xia, M.-W. Mon, K. H. Oh and K.-S. Kim, *Proc. Royal Soc. London Ser. A*, 2012, **468**, 932–953.
42 F. S. Jeng and K. Huang, *J. Struct. Geol.*, 2008, **30**, 633–648.
43 W. Hong, X. Zhao and Z. Suo, *Appl. Phys. Lett.*, 2009, **95**, 111901.
44 E. Hohlfeld and L. Mahadevan, *Phys. Rev. Lett.*, 2011, **106**, 105702.
45 V. Trujillo, J. Kim and R. C. Hayward, *Soft Matter*, 2008, **4**, 564–569.
46 X. Chen and J. Yin, *Soft Matter*, 2010, **6**, 5667–5680.
47 Y. Mei, S. Kiravittaya, S. Harazim and O. G. Schmidt, *Mater. Sci. Eng., R*, 2010, **70**, 209–224.
48 L. A. Taber, *Appl. Mech. Rev.*, 1995, **48**, 487–545.
49 J. Yin, Z. Cao, C. Li, I. Sheinman and X. Chen, *Proc. Natl. Acad. Sci. U. S. A.*, 2008, **105**, 19132–19135.
50 J. Yin, X. Chen and I. Sheinman, *J. Mech. Phys. Solids*, 2009, **57**, 1470–1484.
51 J. Dervaux and M. Ben Amar, *Phys. Rev. Lett.*, 2008, **101**, 68101.
52 A. Goriely and M. Ben Amar, *Phys. Rev. Lett.*, 2005, **94**, 198103.
53 P. D. Shipman and A. C. Newell, *Phys. Rev. Lett.*, 2004, **92**, 168102.
54 C. R. Steele, *J. Appl. Mech.*, 2000, **67**, 237–247.
55 A. Goriely and M. Tabor, *J. Theor. Biol.*, 2003, **222**, 211–218.
56 J. Dumais, S. L. Shaw, C. R. Steele, S. R. Long and P. M. Ray, *Int. J. Dev. Biol.*, 2006, **50**, 209–222.
57 I. B. Heath, *Tip Growth in Plant and Fungal Cells*, Academic Press, New York, 1990.
58 R. Skalak, D. Farrow and A. Hoger, *J. Math. Biol.*, 1997, **35**, 869–907.
59 K. Garikipati, *Appl. Mech. Rev.*, 2009, **62**, 030801.
60 D. Ambrosi and F. Mollica, *Int. J. Eng. Sci.*, 2002, **40**, 1297–1316.
61 J. Humphrey, *Proc. R. Soc. London, Ser. A*, 2003, **459**, 3–46.
62 J. Dunlop, F. Fischer, E. Gamsj ger and P. Fratzl, *J. Mech. Phys. Solids*, 2010, **58**, 1073–1087.
63 E. H. Lee, *J. Appl. Mech.*, 1969, **36**, 1–6.
64 E. K. Rodriguez, A. Hoger and A. D. McCulloch, *J. Biomech.*, 1994, **27**, 455–467.
65 R. Vandiver and A. Goriely, *Europhys. Lett.*, 2008, **84**, 58004.
66 R. W. Ogden, *Non-linear Elastic Deformations*, Courier Dover Publications, New York, 1997.
67 M. A. Biot, *Mechanics of Incremental Deformations*, Wiley, New York, 1965.
68 B. Li, Y. P. Cao, X. Q. Feng and H. Gao, *J. Mech. Phys. Solids*, 2011, **59**, 758–774.
69 E. Efrati, E. Sharon and R. Kupferman, *J. Mech. Phys. Solids*, 2009, **57**, 762–775.
70 R. Luo and H. Li, *Acta Biomater.*, 2009, **5**, 2920–2928.
71 S. Nayak and L. A. Lyon, *Angew. Chem., Int. Ed.*, 2005, **44**, 7686–7708.
72 H. Li, R. Luo, E. Birgersson and K. Y. Lam, *J. Mech. Phys. Solids*, 2009, **57**, 369–382.
73 T. Tanaka, S. T. Sun, Y. Hirokawa, S. Katayama, J. Kucera, Y. Hirose and T. Amiya, *Nature*, 1987, **325**, 796–798.
74 M. K. Kang and R. Huang, *J. Mech. Phys. Solids*, 2010, **58**, 1582–1598.
75 S. Cai, K. Bertoldi, H. Wangab and Z. Suo, *Soft Matter*, 2010, **6**, 5770–5777.
76 W. Hong, Z. Liu and Z. Suo, *Int. J. Solids Struct.*, 2009, **46**, 3282–3289.
77 J. Dervaux and M. Ben Amar, *J. Mech. Phys. Solids*, 2011, **59**, 538–560.
78 M. Ben Amar and P. Ciarletta, *J. Mech. Phys. Solids*, 2010, **58**, 935–954.
79 M. C. Boyce and E. M. Arruda, *Math. Mech. Solids*, 2001, **6**, 641–659.
80 S. A. Chester and L. Anand, *J. Mech. Phys. Solids*, 2010, **58**, 1879–1906.
81 F. P. Duda, A. C. Souza and E. Fried, *J. Mech. Phys. Solids*, 2010, **58**, 515–529.
82 J. Huang, M. Juszkiewicz, W. H. de Jeu, E. Cerda, T. Emrick, N. Menon and T. P. Russell, *Science*, 2007, **317**, 650–653.
83 D. Vella, M. Adda-Bedia and E. Cerda, *Soft Matter*, 2010, **6**, 5778–5782.
84 E. Sharon and E. Efrati, *Soft Matter*, 2010, **6**, 5693–5704.
85 M. Marder and N. Papanicolaou, *J. Stat. Phys.*, 2006, **125**, 1065–1092.

86 E. Efrati, Y. Klein, H. Aharoni and E. Sharon, *Phys. D*, 2007, **235**, 29–32.
87 E. Efrati, E. Sharon and R. Kupferman, *Phys. Rev. E: Stat., Nonlinear, Soft Matter Phys.*, 2009, **80**, 016602.
88 M. Marder, R. D. Deegan and E. Sharon, *Phys. Today*, 2007, **60**, 33–38.
89 Y. Klein, E. Efrati and E. Sharon, *Science*, 2007, **315**, 1116–1120.
90 T. Mora and A. Boudaoud, *Eur. Phys. J. E*, 2006, **20**, 119–124.
91 H. Aharoni and E. Sharon, *Nat. Mater.*, 2010, **9**, 993–997.
92 H. Liang and L. Mahadevan, *Proc. Natl. Acad. Sci. U. S. A.*, 2011, **108**, 5516–5521.
93 A. C. Newell, P. D. Shipman and Z. Sun, *J. Theor. Biol.*, 2008, **251**, 421–439.
94 H. Xiao and X. Chen, *Soft Matter*, 2011, **7**, 10794–10802.
95 Q. Wang, Y. Yin, H. Xie, J. Liu, W. Yang, P. Chen and Q. Zhang, *Soft Matter*, 2011, **7**, 2888–2894.
96 S. Armon, E. Efrati, R. Kupferman and E. Sharon, *Science*, 2011, **333**, 1726–1730.
97 http://en.wikipedia.org/wiki/M%C3%B6bius_strip.
98 A. Korte, E. Starostin and G. van der Heijden, *Proc. R. Soc. London, Ser. A*, 2011, **467**, 285–305.
99 E. Starostin and G. Van der Heijden, *Nat. Mater.*, 2007, **6**, 563–567.
100 T. Witten, *Rev. Mod. Phys.*, 2007, **79**, 643–675.
101 J. Dervaux, P. Ciarletta and M. Ben Amar, *J. Mech. Phys. Solids*, 2009, **57**, 458–471.
102 Z. Liu, W. Hong, Z. Suo, S. Swaddiwudhipong and Y. Zhang, *Comput. Mater. Sci.*, 2010, **49**, S60–S64.
103 N. Stoop, F. K. Wittel, M. Ben Amar, M. M. Muller and H. J. Herrmann, *Phys. Rev. Lett.*, 2010, **105**, 068101.
104 E. Sharon, B. Roman, M. Marder, G. S. Shin and H. L. Swinney, *Nature*, 2002, **419**, 579–579.
105 B. Audoly and A. Boudaoud, *Phys. Rev. Lett.*, 2003, **91**, 86105.
106 E. Sharon, B. Roman and H. L. Swinney, *Phys. Rev. E: Stat., Nonlinear, Soft Matter Phys.*, 2007, **75**, 046211.
107 H. Vandeparre, M. Pineirua, F. Brau, B. Roman, J. Bico, C. Gay, W. Bao, C. N. Lau, P. M. Reis and P. Damman, *Phys. Rev. Lett.*, 2011, **106**, 224301.
108 B. Audoly and Y. Pomeau, *Elasticity and Geometry: From Hair Curls to the Non-linear Response of Shells*, Oxford University Press, 2010.
109 R. D. Schroll, E. Katifori and B. Davidovitch, *Phys. Rev. Lett.*, 2011, **106**, 74301.
110 M. Ortiz and G. Gioia, *J. Mech. Phys. Solids*, 1994, **42**, 531–559.
111 W. Jin and P. Sternberg, *J. Math. Phys.*, 2001, **42**, 192–199.
112 H. Vandeparre, S. Desbief, R. Lazzaroni, C. Gay and P. Damman, *Soft Matter*, 2011, **7**, 6878–6882.
113 J. Huang, B. Davidovitch, C. D. Santangelo, T. P. Russell and N. Menon, *Phys. Rev. Lett.*, 2010, **105**, 38302.
114 C. O. Flynn and B. A. O. McCormack, *Comput. Methods Biomech. Biomed. Eng.*, 2009, **12**, 125–134.
115 L. Landau and E. Lifshitz, *Theory of Elasticity*, Pergammon, Oxford, UK, 1986.
116 N. Bowden, S. Brittain, A. G. Evans, J. W. Hutchinson and G. M. Whitesides, *Nature*, 1998, **393**, 146–149.
117 X. P. Zheng, Y. P. Cao, B. Li, X. Q. Feng, H. Jiang and Y. Y. Huang, *J. Phys. D: Appl. Phys.*, 2009, **42**, 175506.
118 D. Y. Khang, J. Xiao, C. Kocabas, S. MacLaren, T. Banks, H. Jiang, Y. Y. Huang and J. A. Rogers, *Nano Lett.*, 2008, **8**, 124–130.
119 X. P. Zheng, Y. P. Cao, B. Li, X. Q. Feng and G. F. Wang, *Nanotechnology*, 2010, **21**, 205702.
120 B. Audoly and A. Boudaoud, *J. Mech. Phys. Solids*, 2008, **56**, 2422–2443.
121 B. Audoly and A. Boudaoud, *J. Mech. Phys. Solids*, 2008, **56**, 2444–2458.
122 X. Chen and J. W. Hutchinson, *J. Appl. Mech.*, 2004, **71**, 597–603.
123 X. Chen and J. W. Hutchinson, *Scr. Mater.*, 2004, **50**, 797–801.
124 D. Breid and A. J. Crosby, *Soft Matter*, 2011, **7**, 4490–4496.
125 Y. Fung, *Biomechanics: Motion, Flow, Stress, and Growth*, Springer, 1990.
126 A. Goriely, M. Destrade and M. Ben Amar, *Q. J. Mech. Appl. Math.*, 2006, **59**, 615–630.
127 C. A. Hrousis, B. J. R. Wiggs, J. M. Drazen, D. M. Parks and R. D. Kamm, *J. Biomech. Eng.*, 2002, **124**, 334–341.
128 R. Lambert, S. Codd, M. Alley and R. Pack, *J. Appl. Phys.*, 1994, **77**, 1206–1216.
129 B. Li, Y. P. Cao, X. Q. Feng and S. W. Yu, *Appl. Phys. Lett.*, 2011, **98**, 153701.
130 M. H. Fayed, M. Elnasharty and M. Shoaib, *Int. J. Morphology*, 2010, **28**, 111–120.
131 A. Goriely and R. Vandiver, *IMA J. Appl. Math.*, 2010, **75**, 549–570.
132 E. Hannezo, J. Prost and J. F. Joanny, *Phys. Rev. Lett.*, 2011, **107**, 78104.
133 L. Wang, C. L. Pai, M. C. Boyce and G. C. Rutledge, *Appl. Phys. Lett.*, 2009, **94**, 151916.
134 S. K. Basu, a. Alon, V. McCormick and L. Scriven, *Langmuir*, 2006, **22**, 5916–5924.
135 E. Sultan and A. Boudaoud, *J. Appl. Mech.*, 2008, **75**, 051002.
136 H. Jiang, D. Y. Khang, J. Song, Y. Sun, Y. Huang and J. A. Rogers, *Proc. Natl. Acad. Sci. U. S. A.*, 2007, **104**, 15607–15612.
137 B. Audoly, *Phys. Rev. E: Stat., Nonlinear, Soft Matter Phys.*, 2011, **84**, 011605.
138 P. Kim, M. Abkarian and H. A. Stone, *Nat. Mater.*, 2011, **10**, 952–957.
139 L. Pocivavsek, R. Dellsy, A. Kern, S. Johnson, B. Lin, K. Y. C. Lee and E. Cerda, *Science*, 2008, **320**, 912–916.
140 F. Brau, H. Vandeparre, A. Sabbah, C. Poulard, A. Boudaoud and P. Damman, *Nat. Phys.*, 2011, **7**, 56–60.
141 H. Diamant and T. A. Witten, *Phys. Rev. Lett.*, 2011, **107**, 164302.
142 L. Pocivavsek, B. Leahy, N. Holten-Andersen, B. Lin, K. Y. C. Lee and E. Cerda, *Soft Matter*, 2009, **5**, 1963–1968.
143 D. P. Holmes and A. J. Crosby, *Phys. Rev. Lett.*, 2010, **105**, 38303.
144 Y. P. Cao and J. W. Hutchinson, *ASME J. Appl. Mech.*, 2011, in press.
145 E. P. Chan, K. A. Page, S. H. Im, D. L. Patton, R. Huang and C. M. Stafford, *Soft Matter*, 2009, **5**, 4638–4641.
146 R. Huang and Z. Suo, *J. Appl. Phys.*, 2002, **91**, 1135.
147 R. Huang, *J. Mech. Phys. Solids*, 2005, **53**, 63–89.
148 J. Yoon, J. Kim and R. C. Hayward, *Soft Matter*, 2010, **6**, 5807–5816.
149 M. Guvendiren, J. A. Burdick and S. Yang, *Soft Matter*, 2010, **6**, 5795–5801.
150 W. H. Wong, T. F. Guo, Y. W. Zhang and L. Cheng, *Soft Matter*, 2010, **6**, 5743–5750.
151 Y. Cao and J. W. Hutchinson, *Proc. R. Soc. London, Ser. A*, 2012, **468**, 94–115.
152 T. Hwa and M. Kardar, *Phys. Rev. Lett.*, 1988, **61**, 106–109.
153 H. Gao, *J. Mech. Phys. Solids*, 1994, **42**, 741–772.
154 S. Mora, M. Abkarian, H. Tabuteau and Y. Pomeau, *Soft Matter*, 2011, **7**, 10612–10619.
155 P. M. Reis, *Nat. Mater.*, 2011, **10**, 907–909.
156 M. Biot, *Appl. Sci. Res.*, 1963, **12**, 168–182.
157 M. K. Kang and R. Huang, *Soft Matter*, 2010, **6**, 5736–5742.
158 Q. Wang, L. Zhang and X. Zhao, *Phys. Rev. Lett.*, 2011, **106**, 118301.
159 D. E. Moulton and A. Goriely, *J. Mech. Phys. Solids*, 2011, **59**, 525–537.
160 S. Cai, D. Chen, Z. Suo and R. C. Hayward, *Soft Matter*, 2012, **8**, 1301–1304.
161 L. Feng, S. Li, Y. Li, H. Li, L. Zhang, J. Zhai, Y. Song, B. Liu, L. Jiang and D. Zhu, *Adv. Mater.*, 2002, **14**, 1857–1860.
162 X. Q. Feng, X. Gao, Z. Wu, L. Jiang and Q. S. Zheng, *Langmuir*, 2007, **23**, 4892–4896.
163 F. Xia, Y. Zhu, L. Feng and L. Jiang, *Soft Matter*, 2009, **5**, 275–281.
164 J. Yin, E. Bar-Kochba and X. Chen, *Soft Matter*, 2009, **5**, 3469–3474.
165 G. Tomar, D. Bandopadhayay and A. Sharma, *Phys. Rev. E: Stat., Nonlinear, Soft Matter Phys.*, 2011, **84**, 031603.
166 Y. P. Cao, B. Li and X. Q. Feng, *Soft Matter*, 2012, **8**, 556–562.
167 J. Lidmar, L. Mirny and D. R. Nelson, *Phys. Rev. E: Stat. Phys., Plasmas, Fluids, Relat. Interdiscip. Top.*, 2003, **68**, 051910.
168 P. B. Noble, A. R. West, R. A. McLaughlin, J. J. Armstrong, S. Becker, P. K. McFawn, J. P. Williamson, P. R. Eastwood, D. R. Hillman and D. D. Sampson, *J. Appl. Physiol.*, 2010, **108**, 401–411.
169 C. Y. Seow, L. Wang and P. D. Pare, *J. Appl. Physiol.*, 2000, **88**, 527–533.
170 L. Wang, R. Tepper, J. L. Bert, K. L. Pinder, P. D. Pare and M. Okazawa, *J. Appl. Physiol.*, 2000, **88**, 1014–1021.
171 D. E. Moulton and A. Goriely, *J. Appl. Physiol.*, 2011, **110**, 1003–1012.

172 P. Ciarletta and M. Ben Amar, *Int. J. Non-Linear Mech.*, 2011, DOI: 10.1016/j.ijnonlinmec.2011.1005.1013.
173 O. A. Stiennon, *The Longitudinal Muscle in Esophageal Disease*, WRS Press, Wisconsin, 1995.
174 J. C. Hogg, *APMIS*, 1997, **105**, 735–745.
175 J. Dervaux and M. Ben Amar, *IMA J. Appl. Math.*, 2010, **75**, 571–580.
176 J. Yin and X. Chen, *J. Phys. D: Appl. Phys.*, 2010, **43**, 115402.
177 F. Jia, Y. P. Cao and X. Q. Feng, 2011, To be submitted.
178 P. Ciarletta and M. Ben Amar, *J. Mech. Phys. Solids*, 2012, **60**, 525–537.
179 K. Harish and C. Gokulan, *Tropical Gastroenterology*, 2008, **29**, 37–39.
180 R. Vandiver and A. Goriely, *Philos. Trans. R. Soc. London, Ser. A*, 2009, **367**, 3607–3630.
181 R. Martinez, C. Fierro, P. Shireman and H.-C. Han, *Ann. Biomed. Eng.*, 2010, **38**, 1345–1353.
182 A. Rachev, *J. Biomech. Eng.*, 2009, **131**, 051006.
183 R. S. Vannix, E. J. Joergenson and R. Carter, *Am. J. Surg.*, 1977, **134**, 82–89.
184 M. Aleksic, G. Schutz, S. Gerth and J. Mulch, *J. Cardiovasc. Surg.*, 2004, **45**, 43–48.
185 H. C. Han, *J. Biomech.*, 2007, **40**, 3672–3678.
186 H. C. Han, *J. Biomech.*, 2008, **41**, 2708–2713.
187 H. G. Allen, ed., *Analysis and Design of Structural Sandwich Panels*, Pergamon Press, New York, 1969.
188 H. Jiang, D. Y. Khang, H. Fei, H. Kim, Y. Huang, J. Xiao and J. A. Rogers, *J. Mech. Phys. Solids*, 2008, **56**, 2585–2598.
189 S. Tarasovs and J. Andersons, *Int. J. Solids Struct.*, 2008, **45**, 593–600.
190 H. C. Han, *J. Biomech.*, 2009, **42**, 2797–2801.
191 Y. Gerelli, M. T. Di Bari, A. Deriu, D. Clemens and L. Almasy, *Soft Matter*, 2010, **6**, 2533–2538.
192 Y. Lu and M. Ballauff, *Prog. Polym. Sci.*, 2011, **36**, 767–792.
193 K.-H. Hwangbo, M. R. Kim, C.-S. Lee and K. Y. Cho, *Soft Matter*, 2011, **7**, 10874–10878.
194 N. Tsapis, E. R. Dufresne, S. S. Sinha, C. S. Riera, J. W. Hutchinson, L. Mahadevan and D. A. Weitz, *Phys. Rev. Lett.*, 2005, **94**, 018302.
195 E. Katifori, S. Alben, E. Cerda, D. R. Nelson and J. Dumais, *Proc. Natl. Acad. Sci. U. S. A.*, 2010, **107**, 7635–7639.
196 B. Li, F. Jia, Y. P. Cao, X. Q. Feng and H. Gao, *Phys. Rev. Lett.*, 2011, **106**, 234301.
197 R. S. Hill and C. A. Walsh, *Nature*, 2005, **437**, 64–67.
198 P. Tracqui, *Rep. Prog. Phys.*, 2009, **72**, 056701.
199 H. P. Greenspan, *Stud. Appl. Math.*, 1972, **51**, 317–340.
200 R. M. Sutherland, *Science*, 1988, **240**, 177–184.
201 T. Deisboeck, M. Berens, A. Kansal, S. Torquato, A. Stemmer-Rachamimov and E. Chiocca, *Cell Proliferation*, 2001, **34**, 115–134.
202 V. Cristini, H. B. Frieboes, R. Gatenby, S. Caserta, M. Ferrari and J. Sinek, *Clin. Cancer Res.*, 2005, **11**, 6772–6779.
203 K. Pham, H. B. Frieboes, V. Cristini and J. Lowengrub, *J. R. Soc. Interface*, 2011, **8**, 16–29.
204 R. L. MacCarty and N. J. Talley, *Gastrointestinal Radiology*, 1990, **15**, 183–187.
205 H. Jiang and S. X. Sun, *Phys. Rev. Lett.*, 2010, **105**, 28101.
206 L. Wang, C. E. Castro and M. C. Boyce, *Soft Matter*, 2011, **7**, 11319–11324.
207 M. M. Gibbons and W. S. Klug, *J. Mater. Sci.*, 2007, **42**, 8995–9004.
208 G. Vliegenthart and G. Gompper, *New J. Phys.*, 2011, **13**, 045020.
209 W. Roos, R. Bruinsma and G. Wuite, *Nat. Phys.*, 2010, **6**, 733–743.
210 R. Zandi and D. Reguera, *Phys. Rev. E: Stat., Nonlinear, Soft Matter Phys.*, 2005, **72**, 021917.
211 T. Nguyen, R. F. Bruinsma and W. M. Gelbart, *Phys. Rev. E: Stat., Nonlinear, Soft Matter Phys.*, 2005, **72**, 051923.
212 A. Šiber, *Phys. Rev. E: Stat., Nonlinear, Soft Matter Phys.*, 2006, **73**, 061915.
213 A. Šiber and R. Podgornik, *Phys. Rev. E: Stat., Nonlinear, Soft Matter Phys.*, 2009, **79**, 011919.
214 C. Quilliet, C. Zoldesi, C. Riera, A. Van Blaaderen and A. Imhof, *Eur. Phys. J. E*, 2008, **27**, 13–20.
215 M. Buenemann and P. Lenz, *Proc. Natl. Acad. Sci. U. S. A.*, 2007, **104**, 9925–9930.
216 D. Vella, A. Ajdari, A. Vaziri and A. Boudaoud, *Phys. Rev. Lett.*, 2011, **107**, 174301.
217 A. Vaziri and L. Mahadevan, *Proc. Natl. Acad. Sci. U. S. A.*, 2008, **105**, 7913–7918.
218 V. Shenoy and A. Sharma, *J. Mech. Phys. Solids*, 2002, **50**, 1155–1173.
219 J. Sarkar, A. Sharma and V. Shenoy, *Phys. Rev. E: Stat., Nonlinear, Soft Matter Phys.*, 2008, **77**, 031604.
220 S. Herminghaus, *Phys. Rev. Lett.*, 1999, **83**, 2359–2361.
221 B. Li, Y. Li, G. K. Xu and X. Q. Feng, *J. Phys.: Condens. Matter*, 2009, **21**, 445006.
222 E. Schaffer, T. Thurn-Albrecht, T. P. Russell and U. Steiner, *Nature*, 2000, **403**, 874–877.
223 E. Schaffer, T. Thurn-Albrecht, T. P. Russell and U. Steiner, *Europhys. Lett.*, 2001, **53**, 518–524.
224 S. Q. Huang and X. Q. Feng, *Acta Mech. Sin.*, 2008, **24**, 289–296.
225 S. Q. Huang, B. Li and X. Q. Feng, *J. Appl. Phys.*, 2008, **103**, 083501.
226 B. Li, H. P. Zhao and X. Q. Feng, *J. Mech. Phys. Solids*, 2011, **59**, 610–624.
227 C. Q. Ru, *J. Appl. Phys.*, 2001, **90**, 6098–6104.
228 J. Yoon, C. Q. Ru and A. Mioduchowski, *J. Appl. Phys.*, 2005, **98**, 113503.
229 R. Mukherjee, R. C. Pangule, A. Sharma and I. Banerjee, *J. Chem. Phys.*, 2007, **127**, 064703.
230 J. Sarkar, V. Shenoy and A. Sharma, *Phys. Rev. E: Stat. Phys., Plasmas, Fluids, Relat. Interdiscip. Top.*, 2003, **67**, 031607.
231 X. H. Pan, S. Q. Huang, S. W. Yu and X. Q. Feng, *J. Phys. D: Appl. Phys.*, 2009, **42**, 055302.
232 R. Mukherjee, R. Pangule, A. Sharma and G. Tomar, *Adv. Funct. Mater.*, 2007, **17**, 2356–2364.
233 A. Ghatak and M. K. Chaudhury, *Langmuir*, 2003, **19**, 2621–2631.
234 A. Ghatak, M. K. Chaudhury, V. Shenoy and A. Sharma, *Phys. Rev. Lett.*, 2000, **85**, 4329–4332.
235 K. R. Shull, C. M. Flanigan and A. J. Crosby, *Phys. Rev. Lett.*, 2000, **84**, 3057–3060.
236 J. Y. Chung and M. K. Chaudhury, *J. Adhes.*, 2005, **81**, 1119–1145.
237 J. Y. Chung and M. K. Chaudhury, *J. R. Soc. Interface*, 2005, **2**, 55–61.
238 J. Y. Chung, K. H. Kim, M. K. Chaudhury, J. Sarkar and A. Sharma, *Eur. Phys. J. E*, 2006, **20**, 47–53.